Evolution of the eastward shift in the quasi-stationary minimum of the Antarctic total ozone column

Asen Grytsai[1], Andrew Klekociuk[2,3], Gennadi Milinevsky[1,4], Oleksandr Evtushevsky[1], Kane Stone[5,6,*]

[1]Taras Shevchenko National University of Kyiv, 01601 Kyiv, Ukraine

[2]Antarctica and the Global System Program, Australian Antarctic Division, Kingston, Tasmania 7050, Australia

[3]Antarctic Climate and Ecosystems Cooperative Research Centre, Hobart, Tasmania 7000, Australia

[4]Main Astronomical Observatory, National Academy of Sciences of Ukraine, 03143 Kyiv, Ukraine

[5]School of Earth Sciences, University of Melbourne, Melbourne, Victoria 3010, Australia

[6]ARC Centre of Excellence for Climate System Science, University of New South Wales, Sydney, New South Wales 2052, Australia

[*]Currently at the Department of Earth, Atmospheric and Planetary Sciences, Massachusetts Institute of Technology, Cambridge, Massachusetts 02139-4307, USA.

Correspondence to: G. P. Milinevsky (genmilinevsky@gmail.com)

Abstract. The quasi-stationary pattern of the Antarctic total ozone has changed during the last four decades, showing an eastward shift in the zonal ozone minimum. In this work, the association between the longitudinal shift of the zonal ozone minimum and changes in meteorological fields in austral spring (September–November) for 1979–2014 is analysed using ERA-Interim and NCEP–NCAR reanalyses. Regressive, correlative and anomaly composite analyses are applied to reanalysis data. Patterns of the Southern Annular Mode and quasi-stationary zonal waves 1 and 3 in the meteorological fields show relationships with interannual variability in the longitude of the zonal ozone minimum. On decadal time scales, consistent longitudinal shifts of the zonal ozone minimum and zonal wave 3 pattern in the middle troposphere temperature at the southern mid-latitudes are shown. Attribution runs of the ACCESS-CCM chemistry-climate model suggest that long-term shifts of the zonal ozone minimum are separately contributed by changes in ozone depleting substances and greenhouse gases. As is known, Antarctic ozone depletion in spring is strongly projected on the Southern Annular Mode in summer and impacts summertime surface climate across the Southern Hemisphere. The results of this study suggest that changes in zonal

35   ozone asymmetry accompanying ozone depletion could be associated with regional climate changes in the Southern Hemisphere in spring.

40

1 Introduction

The distribution of total column ozone over Antarctica is significantly non-uniform during austral spring, i.e. in September–November (Wirth, 1993; Malanca et al., 2005; Grytsai et al., 2007a;

45   Agosta and Canziani, 2010, 2011). This is particularly the case since the early 1980s due to the presence of ozone depletion associated with the ozone hole (Chubachi, 1984; Farman et al., 1985; Chubachi and Kajiwara, 1986; Stolarski et al., 1986; Solomon, 1999). The total ozone distribution predominantly characterizes the stratosphere layer, where a sharp ozone maximum is usually observed at altitudes of 15–25 km (Chubachi, 1984; Solomon et al., 2005). Therefore, strong

50   variations in the total ozone distribution are due mainly to stratospheric chemistry and dynamics (Wirth, 1993; Gabriel et al., 2011). The ozone hole is located inside polar stratospheric vortex, which is a cyclonic structure that impedes mixing between high-latitude and mid-latitude air masses (Brasseur et al., 1997). The polar vortex is under the influence of large-scale planetary waves, which disturb the vortex edge region (Wirth, 1993; Quintanar and Mechoso, 1995) and the vortex

55   location relative to the pole (Waugh and Randel, 1999). The scale of the waves in the zonal direction is typically characterized by zonal wave number, which equals to the ratio of the corresponding great circle circumference at a given latitude to the wave length (Hirota and Hirooka, 1984; Hio and Yoden, 2004). The stationary part of the wave structure in the Southern Hemisphere (SH) spring stratosphere is mainly determined by a planetary wave with zonal number 1 (Hartmann

60   et al., 1984; Quintanar and Mechoso, 1995; Ialongo et al., 2012), i.e. wave-1. The role of planetary waves was especially important in the unusual SH stratospheric warming in 2002 (Varotsos, 2002; Allen et al., 2003; Hoppel et al., 2003). Both wave-1 and wave-2 activity during austral winter and spring caused strong deceleration and warming of the stratospheric polar vortex, its anomalous splitting and ozone hole breakup in September 2002 (Varotsos, 2002; Nishii and Nakamura, 2004;

65   Newman and Nash, 2005; Peters et al., 2007; Grassi et al., 2008; Peters and Vargin, 2015).

In spring, the ozone distribution in the Antarctic region is asymmetrical with a maximum in the Australian longitudinal sector and a minimum in the Atlantic longitudes (Grytsai et al., 2005; Agosta and Canziani, 2011). Previous studies have revealed the tendency of the Antarctic polar vortex to exhibit an eastward shift in orientation (Huth and Canziani, 2003), in the ozone minimum

70   location (Grytsai et al., 2005; Malanca et al., 2005; Grytsai et al., 2007a, b; Agosta and Canziani, 2010, 2011; Grytsai, 2011; Hassler et al., 2011) and in the phase of wave-1 in stratospheric temperature (Lin et al., 2010). This eastward shift has been described as possibly connected with a change in tropospheric stationary waves (Grytsai et al., 2007a), tropospheric jet structure (Hio and Hirota, 2002; Agosta and Canziani, 2011) and its strengthening (Wang et al., 2013), and

75   stratospheric ozone and volcanic aerosol concentration (Lin et al., 2010). The quasi-stationary wave (QSW) activity increases typically in austral spring (Randel, 1988) and its enhancement leads to larger vortex asymmetry, a decrease in ozone hole area and net stratospheric ozone loss. It has been noted that the decreased (increased) asymmetry in the ozone distribution is associated with the eastward (westward) phase shift of the zonal minimum from both observations at the southern high latitudes

80   (Grytsai et al., 2008; Agosta and Canziani, 2011) and climate model simulations for the northern high latitudes (Gabriel et al., 2007).

It has been revealed that the Antarctic ozone depletion in spring influences the trend in the Southern Annular Mode (SAM) in summer towards the high-index polarity that leads to a range of significant summertime surface climate changes (Thompson et al., 2011). Recent studies have indicated that a

85   stabilization of the spring ozone depletion has occurred from the mid- or late 1990s (Grytsai, 2011; Salby et al., 2011; Kuttippurath et al., 2013; Dameris and Godin-Beekmann, 2014, Solomon et al., 2016). This stabilization relates to the total area of the ozone hole, minimum total ozone values, ozone mass deficit and duration of the ozone hole season. Chemistry-climate models have displayed a general minimum in Antarctic ozone during 2000–2005 (Siddaway et al., 2013) and slow ozone

90   recovery in the 21st century (Dameris and Godin-Beekmann, 2014). In turn, ozone recovery is expected to continue to impact the SH surface climate (Thompson et al., 2011). This work is focused on the recent tendencies in the zonal asymmetry of the Antarctic total ozone in austral spring and their possible relations to the SH atmospheric anomalies.

95

2 Data and methods

In this study, gridded monthly-mean satellite measurements of the total ozone column (TOC) are used to estimate tendencies in the Antarctic quasi-stationary pattern. We restrict our analysis to the September to November (SON) period (austral spring) when the zonal asymmetry in total column

100   ozone is most pronounced. We use measurements from the Total Ozone Mapping Spectrometer (TOMS) / Nimbus-7 (1979–1992), TOMS / Earth Probe (1996–2005) and Ozone Monitoring Instrument (OMI) aboard the Aura platform (2006–2015) which were obtained from the NASA Ozone & Air Quality website http://ozoneaq.gsfc.nasa.gov/. A gap between Nimbus-7 and Earth

Probe observations in 1993–1995 was filled in by Multi Sensor Reanalysis (MSR) data

105 (http://www.temis.nl; van der A et al., 2010).

The original data were obtained with latitude and longitude resolutions of 1° and 1.25°, respectively. We averaged the data over each SON interval to suppress the effects of long-period travelling planetary waves (Grytsai et al., 2007a), and selected zonal values from 50°S to 80°S at 5° latitude intervals; the centres of our selected latitude bins are 50.5°S, 55.5°S, … 80.5°S. The zonal

110 asymmetry in the TOC distribution over this latitude range is illustrated by the OMI measurements in October 2014 (Fig. 1a). Thick white contour in Fig. 1a shows the ozone hole boundary, which corresponds to the threshold TOC value of 220 DU (white line on colour scale in Fig. 1a) defined by the World Meteorological Organization (WMO) criterion (WMO, 2014); see also (Newman et al., 2004) for the rationale for choosing the 220 DU value.

115 Figure 1b shows long-term changes in the zonal TOC asymmetry at 65°S (white circle in Fig. 1a) during SON 1979–2014. In the 2000s (blue curves in Fig. 1b), when ozone loss culminated, zonal TOC minimum is about 100 DU lower than in the pre-ozone hole years (red curves) and is notably displaced to the east. This illustrates a general tendency for the zonal TOC minimum to be located further eastward with decreasing minimum level, as noted previously (Grytsai et al., 2005; Lin et

120 al., 2010; Agosta and Canziani, 2011; Hassler et al., 2011). For the quantitative analysis presented here, the longitudes of the zonal TOC maximum and minimum were determined using a 50-degree window in longitude to separate out the large-scale parts of the disturbances. In this work, long-term tendencies were obtained from polynomial approximation calculated with a least-squares method. The calculations method is described in Supplement 1.

125 Regression, correlation and composite analyses were used to relate the QSW TOC minimum (QSW_{min}) longitude to the meteorological variables. The reliability of the main results is examined comparing the relationships with the two reanalysis data. We use gridded atmospheric variables from the European Centre for Medium-Range Weather Forecasts (ECMWF) reanalysis ERA-Interim (Dee et al., 2011; http://www.ecmwf.int/en/research/climate-reanalysis/era-interim) at

130 1.5°×1.5° (longitude×latitude) resolution and NCEP–NCAR reanalysis (Kalnay et al., 1996; http://www.esrl.noaa.gov/psd/) at 2.5°×2.5° resolution.

3 Results

135

3.1 Longitudinal changes in the QSW structure

First, we compare the long-term changes in total ozone (Fig. 2a) and the longitudinal position of the quasi-stationary ozone minimum (Fig. 2b) at 65°S latitude, which is located in the edge region of

the ozone hole and polar stratospheric vortex (Roscoe et al., 2012) and where the largest QSW amplitude is observed (Grytsai et al., 2007a; Ialongo et al., 2012).

Cubic polynomial fits are shown by thick curves in Fig. 2. These fits are included to highlight the long-term variations in each of the time series and are not done on consideration of any particular underlying physical process. In the early 2000s, the decadal tendencies indicated by the slope of the polynomial fit changed sign in both ozone (from decreasing levels to increasing levels, Fig. 2a) and in ozone minimum longitudes (from eastward shift to westward shift, Fig. 2b). Comparison of polynomials from $k = 2$ to $k = 6$ gives similar opposite tendencies before and after the early 2000s (see Supplement 2, Fig. S1). Note that the quasi-stationary maximum in total ozone at 65°S shows a relatively small decadal shift in longitude (Fig. 2c, thick curve) compared with the level of interannual variability and changes in the QSW_{min} longitude.

On comparing Fig. 2a and 2b, there appears to be some consistency in the epoch of inflexion in the tendencies of both the column amount and the maximum eastward longitude shift of the zonal TOC minimum (around 2000). The eastward shift in the QSW structure over Antarctica has been described previously (Huth and Canziani, 2003; Grytsai et al., 2005, 2007a; Malanca et al., 2005; Agosta and Canziani, 2010, 2011; Lin et al., 2010; Grytsai, 2011; Hassler et al., 2011). Eastward shift speeds of about 15–20°/decade are consistent among various studies (Grytsai et al., 2007a; Lin et al., 2010; Hassler et al., 2011). For the period 1979–2000, the time series in Fig. 2b gives a linear trend of 14.4±12.5°/decade, significant at the 95% level. The westward shift between the early 2000s and early 2010s apparent in Fig. 2b is statistically insignificant and a longer time series is necessary to reliably establish this tendency. Note that Fig. 2b shows large longitude variations during some of the most recent years. Interannual changes in the 2000s and early 2010s covered a wider longitudinal range than in the previous decades. For example, the position of the quasi-stationary minimum was near its extreme western values in 2011 and 2013, whereas it reached the farthest eastern longitude in 2010.

Long-term tendencies in the QSW minimum/maximum longitudes at the seven latitudes between 50°S and 80°S are illustrated in Fig. 3. The extreme longitudinal departures for 1979, 2002 and 2015 relative to the cubic polynomial are shown by closed circles in Fig. 2b. A significant eastward shift of the QSW_{min} from 1979 (solid blue curve) to the early 2000s (dotted blue curve for 2002) by 30–60 degrees of longitude is seen. The curve for 2015 in the region of the zonal TOC minimum (black dotted curve in Fig. 3) is located between the curves for 1979 and 2002 and is shifted westward over the whole zone 50–80°S, i.e. in opposite direction compared with most years of the preceding decade. Changes of the QSW maximum longitudinal position are not regular (Grytsai et al., 2007a) and the largest eastward shifts are seen only at 55°S and 60°S, however, they are not statistically significant due to strong interannual variability (Fig. 2c). The relative stability of the

5

zonal maximum location suggests that higher zonal wave numbers, quasi-stationary wave-2 (QSW2) and wave-3 (QSW3), could be present in the QSW structure, in addition to the dominant quasi-stationary wave-1 (QSW1) (Grytsai et al., 2007a; Agosta and Canziani, 2011).

The two curves in Fig. 4 illustrate the similarity in the interannual variations and decadal changes of the QSW_{min} longitudes and ozone mass deficit in Antarctic spring. The linear correlation between the two variables is positive and r = 0.49–0.57 for the seven latitude circles between 50°S and 80°S with maximum at 60°S. The correlation coefficient r was calculated for the time series length N = 35 (1979–2013, Fig. 4) and the value r = 0.43 is significant at the 99% confidence limit based on a two-tailed Student's t-test. Hence, an eastward shift of the QSW minimum in the ozone distribution with high probability corresponds to a greater ozone mass deficit (larger ozone loss).

Simultaneous negative deviations are observed in the years of large (1988) and major (2002) stratospheric warmings (vertical lines in Fig. 4). Both anomalous events in the SH stratosphere were associated with enhanced planetary wave activity (Varotsos, 2003a; Allen et al., 2003; Baldwin et al., 2003; Grytsai et al., 2008). As seen from Fig. 4, relatively small ozone mass deficits (high total ozone levels) correspond to the westward shift of the QSW_{min} position. Note that this correspondence is not observed in some recent years; the Antarctic spring in 2010 is characterized by eastern longitude of the QSW_{min} at low ozone mass deficit, and the relationship for 2011 is opposite.

The results of Figs. 2–4 show that the eastward shift in the TOC zonal minimum longitude in the Antarctic region was occurred during 1980s–1990s and was accompanied by rapid and intense ozone loss. This decadal tendency appears to have stopped in the early 2000s and became of possibly reverse sign later in the 2000s and 2010s. Generally, the behavior of the zonal TOC minimum in Fig. 2b and Fig. 3 follows the decadal change in the severity of the ozone hole due to international controls on ozone depleting substances (Salby et al., 2011; Solomon et al., 2016), with increasing depletion of the Antarctic ozone in 1980s and 1990s, its leveling off and possible start of recovery in 2000s–2010s (Siddaway et al., 2013). Significant decadal changes in the SH polar ozone are coupled with the stratospheric thermal regime (e.g., Crook et al., 2008) and, because of the zonal asymmetry in the ozone heating, they impact planetary wave propagation (Albers and Nathan, 2012) and regional climate change in both the troposphere and the stratosphere (Gillet et al., 2009; Waugh et al., 2009). Couplings between changes in the QSW structure in Antarctic total column ozone and in atmospheric variables are analyzed below.

3.2 Relationships between the QSW minimum longitude and meteorological parameters

To determine the most reliable mean tendencies, we have created a time series for the QSW_{min}
longitudes averaged between 55°S and 70°S (four latitude circles in Fig. 3); this is shown in Fig. 5.
Bars in Fig. 5 indicate standard deviations for each year and they are generally relatively small
compared with the level of interannual variability in the time series.

We next consider the regression between the time series of Fig. 5 and SON average climatological
anomalies of ERA-Interim meteorological variables. We first produce monthly climatological
anomalies for each gridded monthly average variable at the native horizontal resolution by
subtracting the associated long-term monthly mean (over 1979–2014 for ERA-Interim and 1981–
2014 for NCEP–NCAR). We then produce averages of the anomalies in grid boxes of 10°×10°
(latitude×longitude) over the SON months of each year. Finally, we evaluated the regression
coefficient (RC) between the time series of QSW_{min} longitude of Fig. 5 and the time series of SON
climatological anomalies at each location. Figures 6a and 6b present the global distributions of the
regressions for surface pressure (SP) and 2 metre air temperature (T-2m) over 1979–2014,
respectively. Dots with numbers from 1 to 5 in Fig. 6a are placed at each grid box centre where the
linear correlation coefficient is significant at the 95% confidence limit based on Student's *t*-test
(boxes with significant correlations are also diagonally hatched) and where the fraction of variance
explained (values in %) is ≥ 25% (see text below).

The RC distributions as in Fig. 6a and 6b, but for RC between the QSW_{min} longitude and ERA-
Interim 200-hPa climatological anomalies of zonal wind speed (U200) and vertical pressure wind
speed (W200) are shown in Fig. 6c and 6d, respectively. The pressure level of 200 hPa corresponds
to the upper troposphere in the tropics and lower stratosphere in the SH extratropics and is usually
used to analyze the interaction between the tropics and extratropics (e.g. Mo and Higgins, 1998).
The RC distribution for sea surface temperature (SST) is similar for that for T-2m (Fig. 6b) and the
RC distribution for meridional wind V200 is similar to that for W200 (Fig. 6d), and are not shown
here.

The RC distribution in Fig. 6a shows an annular pattern that is similar to a classic Southern Annular
Mode pattern in SH climate variability, with pressure or geopotential height anomalies of opposite
sign in the middle and high latitudes (Thompson and Wallace, 2000). Negative (positive) regression
coefficients in the high (middle) SH latitudes indicate that the QSW_{min} eastward shift is associated
with decreased (increased) surface pressure, i.e. with the SAM deviation towards positive polarity.

A positive polarity of the annular mode is accompanied by strengthening of the subpolar westerlies
in the SH troposphere and stratosphere and cooling of polar cap regions (Thompson and Wallace,
2000). The RC maximum around 60°S in Fig. 6c and the RC minimum over the Antarctic continent

(poleward of 60°S) in Fig. 6b display similar tendencies in the relationships between the QSW_{min} eastward shift and increase of U200 and decrease of T-2m, respectively.

Zonally asymmetric components of the SH circulation, which are most marked in the austral winter and spring (Mo and Higgins, 1998; Fogt et al., 2012a), are also presented in Fig. 6. Three positive RC anomalies in the SH midlatitudes (grid boxes 1, 2 and 3 in Fig. 6a) demonstrate the presence of a QSW3 structure. The highest negative RC anomaly between grid boxes 2 and 3 is spatially close to the subpolar negative anomaly at grid box 4 and is possibly combined effect of QSW1 and QSW3 (Mo and Higgins, 1998). A significant negative RC anomaly near West Antarctica (grid box 4 in Fig. 6a with an explained variance of 35%) is spatially coincident with the 'pole of variability' in the Amundsen–Bellingshausen Sea Low (ABSL) region (Fogt et al. 2012b and references therein; Turner et al., 2013; Raphael et al., 2016). The midlatitude QSW3 patterns extended to sub-Antarctic latitudes are seen also in the RC distribution for T-2m and W200 (Fig. 6b and 6d, respectively).

The presence of the QSW3 structure in Fig. 6b introduces regional anomalies in the surface temperature distribution. The patterns suggest that when the QSW_{min} moves to the east, surface temperatures are warmer in the Antarctic Peninsula–Weddell Sea region and in the south-west area of Indian Ocean, and cold anomalies appear in the South Pacific and south-east Australia. Hence, variability in zonal asymmetry in the Antarctic ozone during the spring months, with high probability, is indicative of the SH regional climate variability.

Zonal asymmetry in the SH troposphere circulation is closely coupled with the Pacific–South American (PSA) mode (Mo and Higgins, 1998). The PSA pattern in the RC distribution in Fig. 6 is of insignificant intensity, whereas pronounced meridional wave trains are seen in Indian–Australian sector and Atlantic–South American sector (U200 in Fig. 6c). As follows from the relationships below, combined wave activity over the three ocean basins can contribute to the QSW_{min} longitude variability.

All patterns of Fig. 6 are reproduced in correlations with the same variables using the NCEP–NCAR reanalysis data (Supplement 3, Fig. S2) confirming the reliability of the results. In general, Fig. 6 and Fig. S2 show that interannual variations of the SON QSW_{min} longitude during 1979–2014 are associated with the zonally symmetric annular mode and zonally asymmetric QSW structures in the SH atmosphere. In Fig. 7 we present anomaly composites (averages) for years of extreme western (lower 20th percentiles) and eastern (upper 20th percentiles) QSW_{min} longitudes to further investigate the patterns shown in Fig 6. Monthly mean anomalies for September, October and November were calculated by subtraction of the climatological means of 1979–2014 from monthly mean variable value in each grid box as described above concerning Fig. 6. Then monthly mean anomalies were averaged over the SON months.

8

Anomaly composites for the lower 20th percentile of the QSW$_{min}$ longitudes (<−60° longitude, 8 westernmost locations outlined by dashed rectangle in Fig. 5a) are presented in Fig. 7a–7c. Anomaly composites for the higher 80th percentile (>−3.8° longitude, 8 easternmost locations outlined by solid rectangle in Fig. 5a) are presented in Fig. 7d–7f. The years for the westernmost longitudes are 1979, 1980, 1981, 1988, 1990, 2002, 2011 and 2013 (left column of Fig. 7) and the years for the easternmost longitudes are 1985, 1992, 1998, 2001, 2003, 2006, 2008 and 2010 (right column of Fig. 7).

It generally is seen from Fig. 7 that transition from the westernmost longitudes (left column) to the easternmost longitudes (right column) is accompanied by the reversal in the sign of the anomalies. The western (eastern) longitudes correspond to negative (positive) zonal wind anomaly around 60°S in Fig. 7a (7d) and positive (negative) surface pressure poleward of 60°S in Fig. 7b (7e). Opposite anomaly combinations appear in the SH middle latitudes. These changes are consistent with the regression maps in Fig. 6a and 6c, where eastward phase shift indicates similar relationships with U200 (Fig. 6c) and SP (Fig. 6a) displaying the SAM pattern.

Note that the SP anomaly composites show the QSW3-like structure in the SH midlatitudes, which is more intense and shifted to the east in the case of the easternmost QSW$_{min}$ longitudes than in the case of the westernmost longitudes (Fig. 7e and 7b, respectively). The pattern of Fig. 7e means that the regional surface pressure becomes higher in the eastward shifted elements of the QSW3 structure, i.e. deviates to anticyclonic regime in the case of the easternmost QSW$_{min}$ longitudes. The surface pressure growth between the QSW3 anomalies in Fig. 7b and 7e equates to about 8 hPa. Given the seasonal time scale (September–November), this can contribute significantly to regional surface climate change in spring associated with the ozone hole asymmetry change.

The SST anomaly composites demonstrate a relationship of the extreme QSW$_{min}$ longitudes with different tropical regions: western (eastern) longitudes in Fig. 7c (7f) are observed for the negative SST anomalies in the eastern (central) tropical Pacific. The easternmost longitudes in Fig. 7f demonstrate the positive SST anomalies in the western tropical Pacific and in Atlantic, similarly to the same anomaly locations in T-2m in Fig. 6b. Such positive anomaly distributions resemble the pattern of the anomalous SST trend calculated with zonal mean trend removed (Schneider et al., 2015, their Fig. 2f) and the pattern of Atlantic Multidecadal Oscillation (Li et al., 2014; their Fig. 1e).

The SAM, QSW3 and SST patterns seen from Fig. 7 are fully reproduced with the same variables of the NCEP–NCAR reanalysis (Supplement 3, Fig. S3). This is evidence that the QSW$_{min}$ longitudes in the total ozone are steadily coupled with the climate mode (SAM) and stationary wave

structure (QSW3) in the SH atmosphere, as well as with the specific SST anomaly pattern. Further

310   evidence of this coupling is seen from Fig. 8.

Regression of the QSW_{min} longitudes against the SP anomalies at grid box 1 (42.5°S, 65.0°E; Fig. 6a), a mid-latitude element of QSW3, is shown in Fig. 8a. A close similarity can be seen in variations of the SP anomalies in grid box 1 and the QSW_{min} longitudes averaged over 55–70°S: the square of the linear correlation coefficient is $r^2 = 0.57$. In Fig. 8b, time series of the QSW_{min}

315   longitude   and   the   standardized   SAM   index   (Marshall,   2003; https://climatedataguide.ucar.edu/climate-data/marshall-southern-annular-mode-sam-index-station-based) are shown. The square of the linear correlation coefficient between the two time series $r^2 = 0.35$. Therefore, approximately 57% and 35% of the QSW_{min} longitude variance (both significant at the 95% confidence limit) can be explained by the surface pressure anomaly variance described by

320   regional (grid box 1, QSW3 pattern) and hemispheric-scale (SAM) indices, respectively. This indicates that a significant interaction takes place between the identified anomalies in the tropospheric circulation and zonal asymmetry in total ozone (see Section 4 for discussion on the SH troposphere–stratosphere interaction).

As noted from Fig. 6c, the regression coefficient distribution for U200 shows meridional wave

325   trains in the Indian and Atlantic sectors. To contrast the result of Fig. 6c, anomaly composites as in Fig. 7 but for 200 hPa are presented in Fig. 9. Similarly to Fig. 7, transition from the westernmost QSW_{min} longitudes to easternmost ones (left and right columns, respectively) is accompanied by the anomaly sign reversal. The U200 anomaly composites in Fig. 9b and 9f show meridional wave train patterns over the three ocean basins, however, without clear eastward propagation, and it is difficult

330   to determine the wave train sources. Relation of the QSW_{min} longitude to these wave patterns means combined contribution of the QSW sources to the wave structure in the SH stratosphere.

It is important to note the eastward shift of the anomalies between the westernmost and easternmost QSW_{min} longitudes. It can be seen comparing, for example, the QSW1 patterns in T200 at the middle–high SH latitudes (Fig. 9a and 9e) and the QSW3 patterns in W200 at the middle–sub-

335   Antarctic latitudes (Fig. 9c and 9g). Note also more intense anomalies for the easternmost QSW_{min} longitudes in Fig. 9 (right column), which demonstrate lower temperature over large part of the middle–high SH latitudes (T200, Fig. 9e), stronger sub-Antarctic zonal circulation in the lower stratosphere (U200, Fig. 9f) and enhancement of the QSW3 patterns in vertical velocities (W200, Fig. 9g) and eddy heat flux (V'T'200, Fig. 9h). Since the easternmost longitudes characterize mainly

340   1990s and 2000s (as outlined by solid rectangle in Fig. 5), the right column in Fig. 9 could indicate that the two decades of the strongest ozone loss were favorable for the closest interaction between the SAM/QSW3-related anomalies in the SH atmosphere and the QSW structure in total ozone. As

in the case of Fig. 7, the NCEP–NCAR reanalysis shows very similar patterns in the same anomaly composites for 200 hPa (Supplement 3, Fig. S4) confirming the reliability of the results of Fig. 9.

345   In connection between the changes in the QSW structure in total ozone and atmospheric parameters, the clear eastward shift in the QSW3 patterns in the SH midlatitudes (Fig. 7b and 7e and Fig. 9c and 9g) is of particular interest. This tendency is analyzed in more detail using the correlative relationships between the QSW_{min} longitude and air temperature.

3.3 Correlations between the QSW_{min} longitude and the air temperature

350

The linear correlation between time series of the QSW_{min} longitude at 65°S and the ERA-Interim air temperature was evaluated. As the QSW3 structure is concentrated in the mid- and sub-Antarctic latitudes (Figs. 6, 7 and 9), the correlation for air temperature averaged over the zone 40–60°S was calculated. In Fig. 10, the results in the longitude–height cross-section for the 36-year period 1979–

355   2014 are presented. The sample sizes in this case mean that correlation $r = 0.27$ is significant at the 95% confidence limit (black and white contours in Fig. 10 for the positive and negative correlations, respectively).

A clear separation between the QSW1 pattern above the tropopause (peak values of $r \approx \pm 0.7$; climatological thermal tropopause shown by black curve) and the QSW3 pattern below the

360   tropopause ($r_{max} \approx 0.5$) is seen.

The strong correlation in the stratosphere (between 200 hPa and 20 hPa, or 12 km and 26 km, respectively, in Fig. 10), firstly, demonstrates close coupling between the QSW_{min} longitude and the stratospheric temperature in their interannual variations and, secondly, confirms that the QSW_{min} longitude variability is mainly due to the QSW1 contribution. As could be seen from Fig. S5 in

365   Supplement 3, the correlation using the NCEP–NCAR temperature is almost identical to the result of Fig. 10 with the ERA-Interim temperature.

An important feature of the QSW3 pattern in the troposphere is its altitudinal location: the three correlation maxima are located predominantly in the middle troposphere and their peak values are at about 500 hPa (Fig. 10). The correlation is significantly lower at 1000 hPa which could explain

370   relatively weak SST anomalies in the SH midlatitudes in Fig. 7c and 7f. Therefore, the mid-tropospheric pressure level of 500 hPa was chosen for search of possible decadal changes in the correlations between the anomalies in air temperature and in the QSW_{min} longitudes. In Fig. 11, correlation coefficient distributions in a sequence of the five 14-year intervals with the 5–6 year steps are shown. The sample size $N = 14$ and calculated lag-one autocorrelations give significance

375   level of 95% for the correlation coefficient $r = 0.51$.

It is seen that the significant positive correlation peaks (black contours in Fig. 11) shift eastward between 1979–1992 and 1990–2003 by 30–60 degrees (thick lines in Fig. 11a–11c). Later, they

11

remain in average at the easternmost longitudes in 1995–2008 and 2001–2014 (Fig. 11d and 11e, respectively). The QSW3 peak near 180°E exhibits a shift in opposite direction in the last time interval (Fig. 11e). Correlation sequence with the NCEP–NCAR T500 field displays similar tendencies (Supplement 3, Fig. S6).

A significant negative anomaly of the correlation coefficient ($r < -0.5$, white contours) in the South Pacific extending to polar latitudes into the Amundsen–Bellingshausen Sea low (ABSL) region is longitudinally steady (white dashed line). As noted above concerning similar anomaly location in the RC distributions in Fig. 6a and 6b, this could be combined effect of QSW1 and QSW3. Here, meteorological variables in troposphere are correlated with the QSW_{min} longitude in total ozone in their interannual variations, but do not show consistent decadal changes in spatial pattern. Note that annual cycle in the decadal shift of the ABSL longitude could contribute to distinction in zonal shift of the correlation anomalies at the middle and high SH latitudes in Fig. 11. The ABSL shifted westward in average by $-5°$/decade in September–November 1979–2008 (Turner et al., 2013, their Fig. 13) that could partly compensate eastward shift observed in the correlation maxima of the adjoining midlatitudinal zone (Fig. 11).

It can be summarized that common decadal tendencies in total ozone (Fig. 2a), QSW minimum location in the total ozone (Fig. 2b), QSW1 pattern in the lower stratosphere (Fig. 9a and 9e) and QSW3 pattern in the troposphere (Fig. 7b and 7e and Fig. 11) and lower stratosphere (Fig. 9c and 9g) exist. On interannual time scale, the SAM- and QSW1/QSW3-like patterns in the SH circulation associated with variability in the QSW minimum longitude in total ozone are dominating.

In general, the results of Section 3 show that the QSW_{min} longitude changes in the TOC distribution are in statistically significant associations with both the zonal mean (SAM pattern) and regional (QSW1 and QSW3 patterns) anomalies in the spring SH atmosphere. These associations allow us to identify the SH regions, where the climate changes in spring are accompanied by ozone asymmetry changes. Our results, thus, have two differences from known impact of the spring ozone loss on the summer SH climate (Thompson et al., 2011). First, quantitative relationships (Figs. 6–11) are not built on the ozone level changes, but on a spatial parameter, which describes the changes in the location of the zonally asymmetric ozone anomaly (the QSW_{min} longitude). Second, revealed climate signals characterize the Antarctic spring (September–November) and are associated with simultaneous evolution of the ozone hole asymmetry. Possible features of the troposphere–stratosphere interaction, which could contribute to occurrence of revealed links, are discussed below.

4 Discussion

12

The evolution of zonal asymmetry in Antarctic total ozone during 1979–2014 with respect to the changes in the meteorological variables in the SH troposphere and lower stratosphere has been presented in the previous section. Regressive, correlative and anomaly composite analyses show that longitudinal shift of the quasi-stationary zonal TOC minimum has a close relationship with changes in the TOC level itself and with the SAM, QSW and SST patterns. Here we discuss our results in the context of the published literature, including analysis of chemistry-climate model attribution simulations.

4.1 Relation between the TOC asymmetry and TOC level

Analysis covers the austral spring months September–November and the changes in the seasonally averaged longitude of the QSW_{min} characterize the changes in zonal asymmetry of the ozone hole and polar vortex. Zonal asymmetry in the SH stratosphere on monthly and seasonal time scales is formed by prevailing QSW1 that propagates upward from the troposphere (Section 1). In turn, zonal asymmetry in ozone is known to be a factor influencing the planetary wave propagation from the troposphere to the stratosphere (Crook et al., 2008; Albers and Nathan, 2012). Then, the QSW_{min} longitude changes could display changes in both the tropospheric wave sources (their activity and distribution) and modification of the stratospheric QSW through the feedback from zonally asymmetric ozone heating.

The results of this work show that, on interannual and decadal time scales, the QSW_{min} longitudinal location is in close connection with both the QSW_{min} level (Fig. 2b and 2a, respectively) and the overall ozone loss in spring (Fig. 4). Note that ozone mass deficit in Fig. 4 (black curve) characterizes the ozone hole, which is typically asymmetric relative to the South pole. Therefore, the extent of ozone depletion, which is initially depended on the wave activity, appears to be largely coupled with the ozone hole asymmetry. For example, in the years of weak (strong) wave activity in spring, large (low) ozone loss is accompanied by eastward (westward) shift of the QSW_{min}. This is demonstrated by the large simultaneous deviations of the QSW_{min} longitude and ozone mass deficit in 1988 and 2002 (Fig. 4), the years, when enhanced wave activity resulted in the weakened polar vortices and anomalously small ozone holes (Kodera and Yamazaki, 1989; Allen et al., 2003; Varotsos, 2003b; Grassi et al., 2008, Grytsai et al., 2008).

Generally, planetary wave activity contributes significantly to the interannual variability of the ozone hole size, depth and duration (Kodera and Yamazaki, 1989; Allen et al., 2003; Varotsos, 2002, 2004; Ialongo et al., 2012). However, wave activity did not undergo so significant decadal decrease to cause the decadal tendency in ozone depletion and, therefore, can not be contributing factor to the systematic QSW_{min} eastward shift. The long-term loss of Antarctic ozone is attributed to the abundance of ozone-depleting substances (ODS) peaked near the turn of the century (Salby et

13

al., 2011; Dameris and Godin-Beekmann, 2014). Hence, evolution of ODS is initial cause of decadal change in the QSW_{min} level (Fig. 2a). Related change in asymmetric ozone heating that can potentially affect the planetary wave propagation through the feedback processes (Crook et al., 2008; Albers and Nathan, 2012) could also result in the QSW structure modification. Consistent decadal tendencies seem to support assumption that evolution of zonally asymmetric ozone depletion (Fig. 2a) could be main cause of the QSW_{min} shift (Fig. 2b). Note that decadal changes of the ozone hole metrics seem to be also influenced by ozone depletion itself. For example, the delay in the final warming of the Antarctic vortex and seasonal disappearance of the ozone hole in 1980s–1990s appears influenced by increasing overall ozone loss (Haigh and Roscoe, 2009).

Thus, interaction between the planetary waves and ozone could underlay observed evolution of the asymmetric ozone hole: (i) zonal asymmetry in Antarctic ozone is initially induced by the QSW propagating from the troposphere, (ii) significant change in the TOC level occurs within asymmetric ozone hole causing change in zonally asymmetric ozone heating that, (iii) through the feedback processes, could result in the QSW structure modification.

4.2 The SAM pattern

As it is known, positive SAM polarity is associated with the enhanced westerlies around Antarctica and decreased surface pressure and air temperature in the polar region (Thompson and Wallace, 2000). The eastward shift of the QSW minimum in total ozone is accompanied by similar indications of the positive SAM polarity: strengthening of zonal wind around Antarctica (U-10m in Fig. 7d and U200 in Fig. 9f), surface pressure decrease (SP in Fig. 7e) and air temperature decrease (T-200 in Fig. 9e and T500 in Fig. 11) in the SH high latitudes.

Our results do not give information on the direction of the 'QSW_{min}–SAM' coupling. Tropospheric circulation disturbances can influence the evolution of the stratospheric polar vortex and, in turn, stratospheric processes can induce a tropospheric response that projects on the annular mode (Thompson ans Wallace, 2000). It is known that the Antarctic ozone losses in spring impact the SAM-related tropospheric circulation predominantly in summer (Thompson et al., 2011; Schneider et al., 2015) and the spring SAM index shows near-zero decadal trend (Marshall, 2003; Fogt et al., 2009; Arblaster and Gillett, 2014). In addition, in our relationships for zonal wind (Fig. 7a and 7d and Fig. 9b and 9f), it is difficult to reveal evidence of the poleward shift of the westerly jets observed usually in the positive SAM polarity (Thompson and Wallace, 2000). This is because of strong disturbance of zonal anomaly orientation by the midlatitude QSW3 structure. So, on decadal time scale, influence of the ozone change accompanied by the QSW_{min} longitude change (Fig. 2a and 2b, respectively) on the spring SAM pattern can not be identified from our results.

Nevertheless, such feedback possibility can not be fully excluded, at least on interannual time scales. As shown by Son et al. (2013), stratospheric ozone concentration in September is strongly correlated with the SAM index in October with $r = -0.7$. The mechanism of this time-lagged downward coupling remains to be determined.

Thus, the appearance of the SAM-like patterns in our relationships (Fig. 6, Fig. 7 and Fig. 9) can be interpreted in two ways that are influenced by interannual variability: first, the strength and pattern of the circulation in the spring SH troposphere can conceivably play a significant role in determining the location of the QSW structure in the stratosphere, and, second, the QSW structure in the stratosphere can potentially provide a downward influence on the tropospheric circulation. This could mean that assumed feedback processes of the asymmetric ozone loss (noted in Section 4.1 with respect to the QSW structure in the stratosphere) may spread into the troposphere in the springtime. The results by Son et al. (2013) demonstrate such possibility using ozone index for the SH polar area. However, ozone variability in the SH polar area is typically combined with the ozone asymmetry variability (Fig. 2) and combined effect of the ozone itself and ozone asymmetry could affect the interannual variability of SH surface climate in spring noted in (Son et al., 2013).

4.3 The QSW1/QSW3 patterns

Unlike the SAM pattern, the atmospheric QSW3 pattern in the midlatitude troposphere demonstrates long-term changes (Fig. 11) consistent with both the ozone loss tendency (Fig. 2a and Fig. 4, black curve) and the QSW_{min} longitude shift (Fig. 2b). Positive correlations of up to $r = 0.7$–0.8 and the longitudinal shift of the three correlation maxima in Fig. 11 are evidence of significant coupling between QSW_{min} and QSW3 on both interannual and decadal time scales. QSW3, although smaller than QSW1, is a dominant feature of the SH midlatitude circulation on daily, seasonal and interannual timescales (Raphael, 2004, and references therein). The QSW3 ridges determined from the 500-hPa geopotential height anomalies over the period 1958–2001 by Raphael (2004) are located climatologically over southern South America, the southern Indian Ocean and southwest of New Zealand.

Those ridge locations correspond to the correlation maxima in Fig. 11a and 11b for the periods 1979–1992 and 1984–1997, respectively, which cover the last two decades of the time interval in Raphael (2004). The largest eastward shift of the QSW3 pattern occurred between the 1980s and 1990s (Fig. 11a and 11c, respectively). The central ridge that is located on average near 180°E (Fig. 10) drifted from the southwest of New Zealand in the 1980s (as in Raphael (2004) and shown in Fig. 11a) to southeast of New Zealand by the early 2000s (Fig 11d), covering over about 60° of longitude. Apparent in the longitude sector of this ridge in the 1990s and 2000s has been a cooling of the tropical central Pacific that has been linked to wind-driven vertical circulation changes in the

Pacific Ocean (England et al., 2014); this process is also associated with the spin-up of the subtropical gyres and associated surface ocean warming (see Fig. 2 of England et al. (2014)) in the region of the ridge. In the 2000s and 2010s, as seen from Fig. 11c–11e, the ridge locations showed less drift. In particular, Figure 11e indicates that the central ridge has drifted west back towards New Zealand.

Note that in the years of maximum ozone hole area (easternmost QSW_{min}), the midlatitude wave 3 anomalies of the positive correlation partly cover New Zealand and southern tip of South America (Fig. 11c–11e, and Fig. S6c–S6e). Positive anomaly here corresponds to climate warming in the years of the easternmost QSW_{min} migrations. In future, predicted ozone recovery may be accompanied by further westward shift of the wave 3 pattern and by weakening of the positive anomaly influence in region of New Zealand and South America (similarly to Fig. 11a and Fig. S6a).

As seen from Fig. 11a and Fig. S6a, both reanalyses show negative correlation anomalies over Australia and East Antarctica in the first time interval 1979–1992 (pre-ozone hole and first ozone hole years, westernmost QSW_{min},). Later, these negative anomalies weaken (Fig. 11b–11d) and appear again in the latest time interval 2011–2014 (Fig. 11e). Note that regression in Fig. 6b and correlation in Fig. S2b also show negative anomaly over south-east part of Australia. These tendencies indicate that Antarctic ozone recovery to pre-ozone hole level may be accompanied by strengthening of negative coupling 'tropospheric temperature – QSW_{min} longitude' in this region. All of these climate effects need further analysis.

The QSW1 structure in the lower stratosphere covers the middle and high SH latitudes, and, in the two reanalyses, shows consistent eastward shift between the westernmost and easternmost locations of the QSW_{min} (Fig. 9a and 9e; Fig. S4a and S4c). Note that the QSW1 pattern in Fig. 10 takes the altitude range where vertical ozone profile in the austral spring undergoes the largest ozone decrease (Chubachi, 1984; Varotsos, 2003b; Solomon et al., 2005). Dynamical activity changes the extent of ozone depletion from year to year and, in the conditions of zonal asymmetry of the polar vortex, enhances the TOC variability. The role of zonal asymmetry becomes more important due to vertical non-alignment of the vortex structure (Varotsos, 2004). The vortex appears progressively shifted with height towards South America and high ozone in the middle stratosphere (around 30 km) within the Australian sector masks ozone depletion in the lower stratosphere (Kondragunta et al., 2005; Tully et al., 2008) resulting in additional variability of stratospheric temperature, column ozone and ozone hole characteristics. In this way, vertical changes in the QSW1 structure impact the ozone profile over Antarctica and contribute to the strong correlation between zonal asymmetry in ozone distribution (QSW_{min} longitude) and stratospheric temperature in Fig. 10.

16

Overall, the long-term shifts in the QSW3 centers and the QSW1 pattern show a temporal evolution that is qualitatively similar to decadal changes in both ozone depletion (Fig. 2a and Fig. 4, black curve) and the shift of QSW_{min} in total ozone (Fig. 2b). This similarity suggests that decadal-scale changes in the QSW structures in the troposphere and stratosphere could either have independent common source, or result from troposphere–stratosphere interaction in the SH extratropics including feedback processes assumed in Sections 4.1 and 4.2. Both possible mechanisms deserve further analysis using observational data and models.

Simulated influence of the greenhouse gases increase on the eastward phase shift in the stratospheric stationary waves (Wang et al., 2013) indicates the possible contribution of the first mechanism. This model simulation links eastward phase shift to the strengthening of the subtropical jet driven by greenhouse gases forcing via sea surface warming. Induced eastward shift is projected by the model to the end of the 21st century (Wang et al., 2013).

Agosta and Canziani (2011) have shown that there are significant interactions/coupling between the ozone layer, the troposphere, and the stratosphere during the austral spring, which can be traced by the phase changes in TOC and QSW1 in the stratosphere. Such changes and troposphere–stratosphere interactions, by Agosta and Canziani (2011), are linked to both the upward and downward propagation of quasi-stationary wave anomalies. Taking into account the results by Son et al. (2013) and the results of our work, the second of the mentioned mechanisms that suggests contribution of ozone change may be more effective in the recent decades.

4.4 The SST patterns

Clear difference between the SST anomaly patterns for the westernmost and easternmost QSW_{min} locations has been identified using the two reanalysis data (Fig. 7c and 7f; Fig. S3c and S3f). Particularly, the westernmost locations show the negative SST anomaly in the eastern tropical Pacific (La Niña type anomaly; more intense in the NCEP–NCAR reanalysis than in ERA-Interim, Fig. S3c and Fig. 7c, respectively). The westernmost locations show the negative SST anomaly in the central tropical Pacific (Fig. 7f and Fig. S3f).

Difference between the two regions of the tropical Pacific in their coupling with the QSW structure in the SH stratosphere was noted by Lin et al. (2012). By Lin et al. (2012), westward QSW phase shift is seen for negative SST anomalies (La Niña events) in the eastern Pacific and eastward shift is seen for warm SST anomalies in the central Pacific. The results of Fig. 7c and Fig. S3c show a similar association between the westernmost QSW_{min} longitudes and negative SST anomaly in the eastern Pacific. However, the easternmost longitudes in Fig. 7f and Fig. S3f show also a negative anomaly in the central Pacific, as distinct from a positive one (Lin et al., 2012).

17

585   In the individual years, large westward phase shift in the QSW_{min} occurred in 1988 and 2002 (Fig. 2b and Fig. 4). Sources of anomalous planetary waves in these years have been identified in both the tropical Pacific (Kodera and Yamazaki, 1989; Grassi et al., 2008) and the SH extratropics (Nishii and Nakamura, 2004; Peters et al., 2007). It has been noted that the evolutions of sea surface temperatures in the tropical Pacific in the spring months of 1988 and 2002 were different (Varotsos

590   et al., 2003b) with strong La Niña and emerging El Niño conditions, respectively (McPhaden, 2004; see   also   time   series   for   the   indices   Niño   3   and   Niño   4   at http://www.esrl.noaa.gov/psd/data/climateindices/).

In the case of 2002 this is counter to the expectation from Lin et al. (2012) based on the prevailing positive central Pacific SST anomaly (McPhaden, 2004) and disagrees with Fig. 7f and Fig. S3f,

595   since a negative SST anomaly exists in this region.

Note that Fig. 7f and Fig. S3f show a significant negative SST anomaly in the South Pacific and positive SST anomalies in the western tropical Pacific and in the Atlantic. Similarly to the PSA mode in the Pacific sector, poleward propagating Rossby wave train could be driven by the Atlantic SST anomalies (e.g., Li et al., 2014). Combined influences of the wave train could result in other

600   phase shift direction in the SH stratosphere planetary waves than from positive anomaly in the central tropical Pacific in (Lin et al., 2012). In particular, the SH extratropical Rossby wave activity that propagated into the stratosphere in the spring of 2002 (Nishii and Nakamura, 2004; Peters et al., 2007) could also have contributed to the observed QSW_{min} shift in that year.

In general, the results of Section 3 reveal indications of the connection between changes in zonal

605   asymmetry in Antarctic total ozone and changes in zonally symmetric (SAM) and zonally asymmetric (QSW1 and QSW3) patterns in the SH circulation, as well in the SST patterns. These results are, in general, in agreement with known evidence of coupling between Antarctic ozone and SAM (Thompson and Wallace, 2000; Waugh et al., 2009; Thompson et al., 2011), the SH QSW structure (Agosta and Canziani, 2011; Wang et al., 2013) and the SSTs (Kodera and Yamazaki,

610   1989; Grassi et al., 2008). These couplings allow us to identify the SH regions, where the climate changes in spring are accompanied by the ozone asymmetry changes.

4.5 Attribution of longitude shift

We now turn to chemistry-climate model simulations to further examine long-term changes in the

615   QSW pattern. Here we consider simulations for the Chemistry-Climate Model Initiative (CCMI) (Eyring et al., 2013) produced by the chemistry-climate version of the Australian Community Climate and Earth System Simulator (ACCESS-CCM; Stone, 2015; Stone et al., 2016). Specifically, we examine single simulations from the REF-C2, SEN-C2-fODS and SEN-C2-fGHG scenarios which are described in detail by Stone (2015). The REF-C2 simulation covers the period

620   1960–2100 and includes evolving concentrations of greenhouse gases (GHGs) and Ozone Depleting
       Substances (ODSs); the SEN-C2-fODS and SEN-C2-fGHG simulations are similar to REF-C2
       except that ODSs and GHGs, respectively, are separately fixed at 1960 levels.

       The ACCESS-CCM simulations favorably reproduce general characteristics of ozone depletion and
       stratospheric stationary waves compared with observations and various similar models (Stone,
625   2015; Stone et al., 2016). In Fig. S7a of Supplement we show the meridional cross-section of the
       correlation between temperature and QSW_{min} longitude for the REF-C2 simulation over 1979–2014
       for direct comparison with Fig. 10. Although the strength of the correlations in the REF-C2
       simulations (Fig. S7a) is weaker than seen in the ERA-Interim reanalysis (Fig. 10) and in the
       NCEP–NCAR reanalysis (Fig. S5), the simulation shows similarly located patterns; for example,
630   the region of positive correlation in the lower stratosphere is of similar extent as in the reanalyses,
       but shifted ~30° westward for the REF-C2 simulation. Correlation analysis for an additional model
       simulation, REF-C1, over 1979–2010, which has a similar setup to REF-C2 (Stone, 2015), shows in
       Fig. S7b a closer agreement with Fig. 10 and Fig. S5 and we conclude that model internal
       variability has a noticeable influence on the correlations on these timescales.

635   Stone (2015) has investigated the long-term shift in the Southern Hemisphere TOC patterns in
       spring and summer in relation to GHG and ODS changes, where the phase of the wave-1
       component of the TOC (obtained from a zonal Fourier decomposition) was analyzed in a similar
       manner to Grytsai et al. (2007a). By regressing the wave phase against measures of GHG and ODS
       forcing, Stone (2015) finds that ODS forcing explains a significant fraction of the long-term
640   variability in the wave-1 longitude compared with GHG in spring at 50°S and 60°S (his Fig. 5.6),
       with the strongest influence at the equatorward latitude. From examining also the wave-1 pattern in
       temperature at 50 hPa and 500 hPa and zonal wind at 10 hPa, Stone (2015) concludes that
       temperature changes associated with the spring ozone depletion play the most important role in the
       eastward shift of the TOC pattern at these latitudes, whereas influences from GHG changes are
645   mitigated by a blocking effect from the continental features, particularly the Andes. As noted in
       Section 4.3, simulated GHG increase during the 21st century shows the eastward phase shift in the
       stratospheric stationary waves and this shift is linked to the strengthening of the subtropical jet
       driven by greenhouse gases forcing via sea surface warming (Wang et al., 2013).

       While Stone (2015) only examined the wave-1 phase, we show in Fig. 12 long-term trends in
650   QSW_{min} from the REF-C2, SEN-C2-fODS and SEN-C2-fGHG simulations averaged over 55°S to
       70°S, as well as the observational data presented in Fig. 5. While there is large interannual
       variability, the SEN-C2-fGHG run (which has evolving ozone changes and fixed GHG level), and
       to a lesser extent the REF-C2 run (which has both evolving GHG and ODS changes) both show a
       tendency for an eastward shift (peaking around 2000–2025) and then westward relaxation over the

655 ozone hole period (to about 2060). On the other hand, the SEN-C2-fODS simulation in which GHGs evolve, shows a much smaller trend and overall less variability over the ozone hole period compared with the other simulations. We note that while the observations show a mean phase shifted ~30–40° further east than the simulations (similar to the difference noted between the positive correlation in the lower stratosphere between Figs. 10 and S7), the variability in the

660 observational record is not dissimilar to the variability on similar time scales in the simulations.

Overall we conclude from the simulations that ozone depletion is providing a strong influence on the QSW_{min} phase in the current period, and may be playing an important role in the level of interannual variability in the stratospheric quasi-stationary wave pattern, and possibly also the pattern in the troposphere, at least over latitudes around 60°S.

665

5 Conclusions

We have examined the variability of the minimum in the quasi-stationary pattern in total column ozone in spring at high southern latitudes using observations and model simulations. Our main results are:

670 1) In interannual variations, the longitude of the QSW minimum in total ozone is in close association with the SAM index, the QSW1/QSW3 patterns in the meteorological variables and the SST patterns. Particularly, easternmost (westernmost) longitudes of the QSW minimum are accompanied by shift of the SAM index to positive (negative) polarity (Fig. 8b).

2) On the decadal time scale, a consistency between the longitudinal shifts of the QSW minimum in

675 total ozone (Fig. 2b) and the QSW3 pattern in the mid-tropospheric temperature (Fig. 11) has been shown.

3) The SST anomalies over the Pacific and Atlantic basins contribute to the variability in the QSW minimum location.

4) Based on the results from our attribution experiments with the ACCESS-CCM climate model,

680 increased levels of ODS and GHGs both tend to shift the QSW_{min} eastward. From the simulations, asymmetric ozone depletion in spring is likely having a strong influence on the phase of the stratospheric wave pattern around 60°S.

Regression, correlation, anomaly composite and model analyses show that longitudinal variability in location of the quasi-stationary zonal TOC minimum has a close relationship with variability in

685 the TOC level itself, in the SAM/QSW patterns in the meteorological variables and in the SST patterns. Therefore, these couplings allow us to identify the SH regions, where the climate variability and climate change in austral spring could be accompanied by the ozone hole asymmetry changes. Related shifts in the tropospheric QSW3 pattern play a role in climate variability in regions of Australia, New Zealand and southern tip of South America. On the one hand, the results

20

690   suggest combined influences of the QSW sources on the stationary wave structure in the SH stratosphere and, on the other hand, they indicate possible ozone change feedback affecting the wave structure.

Chemistry-climate models predict that the Antarctic ozone will return to the 1980 level in the second half of the 21st century, in 2050–2070 period (Siddaway et al., 2013; Dameris and Godin-

695   Beekmann, 2014; Solomon et al., 2016) and the period of ozone recovery will take approximately 3 times longer than did the growth epoch of the ozone hole (approximately 2000–2060 and 1980s–1990s, respectively). From our simulations, recovery in ozone levels during the next 2–3 decades will allow the QSW$_{min}$ location to generally reverse direction and drift westwards, until the forcing by increasing GHGs starts to dominate and eastward drift resumes (after approximately 2060). The

700   combined impacts of the decadal changes in ozone and GHG on the SH stationary waves indicated by our results suggest that surface influences can be expected over the remainder of this century. It is also possible that interannual variability in the stratospheric stationary waves may reduce as ozone depletion subsides, and this may also have a bearing of interannual variability in high latitude surface climate. Further model evaluations are needed to assess these indications.

705

Author contribution

Based on ideas developed by G. P. M., A. V. G. performed data development and provided analysis with contribution from G. P. M., A. R. K., O. M. E and K. A. S. G. P. M., A. R. K. and O. M. E. provided additional explanation of the outputs. A. V. G. prepared the manuscript with contributions

710   from G. P. M., A. R. K. and O. M. E.

References

Agosta, E. A. and Canziani, P. O.: Interannual variations in the zonal asymmetry of the subpolar latitudes total ozone column during the austral spring, GeoActa, 35, 1–16. 2010.

Agosta, E. A. and Canziani, P. O.: Austral spring stratospheric and tropospheric circulation interannual variability, J. Climate, 24, 2629–2647, doi:10.1175/2010JCLI3418.1, 2011.

Albers, J. R. and Nathan, T. N.: Pathways for communicating the effects of stratospheric ozone to the polar vortex: Role of zonally asymmetric ozone, J. Atmos. Sci., 69, 785–801, doi:10.1175/JAS-D-11-0126.1, 2012.

Allen, D. R., Bevilacqua, R. M., Nedoluha, G. E., Randall, C. E., and Manney, G. L.: Unusual stratospheric transport and mixing during the 2002 Antarctic winter, Geophys. Res. Lett., 30, 1599, doi:10.1029/2003GL017117, 2003.

Arblaster, J. M., Gillett, N. P. (Lead Authors), Calvo, N., Forster, P. M., Polvani, L. M., Son, S.-W., Waugh, D. W., and Young, P. J.: Stratospheric ozone changes and climate, Chapter 4 in Scientific Assessment of Ozone Depletion: 2014, Global Ozone Research and Monitoring Project – Report No. 55, World Meteorological Organization, Geneva, Switzerland, 2014.

Baldwin, M., Hirooka, T., O'Neill, A., and Yoden, S.: Major stratospheric warming in the Southern Hemisphere in 2002: Dynamical aspects of the ozone hole split, SPARC Newsletter, 20, 24–27, http://www.sparc-climate.org/publications/newsletter/, 2003.

Brasseur, G. P., Tie, X. X., Rasch, Ph. J., and Lefèvre, F.: A three-dimensional simulation of the Antarctic ozone hole: Impact of anthropogenic chlorine on the lower stratosphere and upper troposphere, J. Geophys. Res., 102, 8909–8930, doi:10.1029/96JD03398, 1997.

Chubachi, S.: Preliminary result of ozone observations at Syowa station from February 1982 to January 1983, Mem. Natl. Inst. Polar Res., Spec. Issue Jpn., 34, 13–19, 1984.

Chubachi, S. and Kajiwara, R.: Total ozone variations at Syowa, Antarctica, Geophys. Res. Lett., 13, 1197–1198, doi:10.1029/GL013i012p01197, 1986.

Crook, J. A., Gillett, N. P., and Keeley, S. P. E.: Sensitivity of Southern Hemisphere climate to zonal asymmetry in ozone, Geophys. Res. Lett., 35, L07806, doi:10.1029/2007GL032698, 2008.

Dameris, M., and Godin-Beekmann, S. (Lead Authors), Alexander, S., Braesicke, P., Chipperfield, M., de Laat, A. T. J., Orsolini, Y., Rex, M., and Santee, M. L.: Update on polar ozone: Past, present, and future, Chapter 3 in Scientific Assessment of Ozone Depletion: 2014, Global Ozone Research and Monitoring Project − Report No. 55, World Meteorological Organization, Geneva, Switzerland, 2014.

Dee, D. P., Uppala, S. M., Simmons, A. J., Berrisford, P., Poli, P., Kobayashi, S., Andrae, U., Balmaseda, M. A., Balsamo, G., Bauer, P., Bechtold, P., Beljaars, A., van de Berg, L., Bidlot, J., Bormann, N., Delsol, C., Dragani, R., Fuentes, M., Geer, A. J., Haimberger, L., Healy, S. B., Hersbach, H., Hólm, E. V., Isaksen, L., Kallberg, P., Köhler, M., Matricardi, M., McNally, A. P., Monge-Sanz, B. M., Morcrette, J.-J., Park, B. K., Peubey, C., de Rosnay, P., Tavolato, C., Thépaut, J.-N., and Vitart, F.: The ERA-Interim reanalysis: configuration and performance of the data assimilation system, Q. J. Roy. Meteorol. Soc., 137, 553–597, doi:10.1002/qj.828, 2011.

England, M. H., McGregor, S., Spence, P., Meehl, G.A., Timmermann, A., Cai, W., Sen Gupta, A., McPhaden, M. J., Purich, A. and Santoso, A.: Recent intensification of wind-driven circulation in the Pacific and the ongoing warming hiatus, Nature Climate Change, 4, 222–227, doi:10.1038/nclimate2106, 2014.

Eyring, V., Lamarque, J.-F., Hess, P., Arfeuille, F., Bowman, K., Chipperfield, M. P., Duncan, B., Fiore, A., Gettelman, A., Giorgetta, M. A., Granier, C., Hegglin, M., Kinnison, D., Kunze, M., Langematz, U., Luo, B., Martin, R., Matthes, K., Newman, P. A., Peter, T., Robock, A., Ryerson, T., Saiz-Lopez, A., Salawitch, R., Schultz, M., Shepherd, T. G., Shindell, D., Staehelin, J., Tegtmeier, S., Thomason, L., Tilmes, S., Vernier, J.-P., Waugh, D., and Young, P. Y.: Overview of IGAC/SPARC Chemistry-Climate Model Initiative (CCMI) community simulations in support of upcoming ozone and climate assessments, SPARC Newsletter, 40, 48–66, 2013.

Farman, J. C., Gardiner, B. G., and Shanklin, J. D.: Large losses of total ozone in Antarctica reveal seasonal ClOx/NOx interaction, Nature, 315, 207–210, doi:10.1038/315207a0, 1985.

Fogt, R. L., Jones, J. M., and Renwick, J.: Seasonal zonal asymmetries in the Southern Annular Mode and their impact on regional temperature anomalies, J. Climate, 25, 6253–6270, doi:10.1175/JCLI-D-11-00474.1, 2012a.

Fogt, R. L., Wovrosh, A. J., Langen, R. A., and Simmonds, I.: The characteristic variability and connection to the underlying synoptic activity of the Amundsen-Bellingshausen Seas Low, J. Geophys. Res., 117, D07111, doi:10.1029/2011JD017337, 2012b.

Fogt, R. L., Perlwitz, J., Monaghan, A. J., Bromwich, D. H., Jones, J. M., and Marshall, G. J.: Historical SAM variability. Part II: Twentieth-century variability and trends from reconstructions, observations, and the IPCC AR4 models, J. Climate, 22, doi:10.1175/2009JCLI2786.1, 5346–5365, 2009.

Gabriel, A., Körnich, H., Lossow, S., Peters, D. H. W., Urban, J., and Murtagh, D.: Zonal asymmetries in middle atmospheric ozone and water vapour derived from Odin satellite data 2001–2010, Atmos. Chem. Phys., 11, 9865–9885, doi:10.5194/acp-11-9865-2011, 2011.

Gabriel, A., Peters, D., Kirchner, I., and Graf, H.-F.: Effect of zonally asymmetric ozone on stratospheric temperature and planetary wave propagation, Geophys. Res. Lett., 34, L06807, doi:10.1029/2006GL028998, 2007.

Gillett, N. P., Scinocca, J. F., Plummer, D. A., and Reader, M. C.: Sensitivity of climate to dynamically consistent zonal asymmetries in ozone, Geophys. Res. Lett., 36, L10809, doi:10.1029/2009GL037246, 2009.

Grassi, B., Redaelli, G., and Visconti, G.: Tropical SST preconditioning of the SH polar vortex during winter 2002, J. Climate, 21, 5295–5303, doi: 10.1175/2008JCLI2136.1, 2008.

Grytsai, A.: Planetary wave peculiarities in Antarctic ozone distribution during 1979–2008, Int. J. Remote Sens., 32, 3139–3152, doi:10.1080/01431161.2010.541518, 2011.

Grytsai, A., Grytsai, Z., Evtushevsky, A., and Milinevsky, G.: Interannual variability of planetary waves in the ozone layer at 65° S, Int. J. Remote Sens., 26, 3377–3387, doi:10.1080/01431160500076350, 2005.

Grytsai, A. V., Evtushevsky, O. M., Agapitov, O. V., Klekociuk, A. R., and Milinevsky, G. P.: Structure and long-term change in the zonal asymmetry in Antarctic total ozone during spring, Ann. Geophys., 25, 361–374, doi:10.5194/angeo-25-361-2007, 2007a.

Grytsai, A., Evtushevsky, A., Milinevsky, G., and Agapitov, A.: Longitudinal position of the quasi-stationary wave extremes over the Antarctic region from the TOMS total ozone, Int. J. Remote Sens., 28, 1391–1396, doi:10.1080/01431160600768021, 2007b.

Grytsai, A. V., Evtushevsky, O. M., and Milinevsky, G. P.: Anomalous quasi-stationary planetary waves over the Antarctic region in 1988 and 2002, Ann. Geophys., 26, 1101–1108, doi:10.5194/angeo-26-1101-2008, 2008.

Haigh, J. D. and Roscoe H. K.: The final warming date of the Antarctic polar vortex and influences on its interannual variability, J. Climate, 22, 5809–5819, doi:10.1175/2009JCLI2865.1, 2009.

825 Hartmann, D. L., Mechoso, C. R., and Yamazaki, K.: Observations of wave-mean flow interaction in the Southern Hemisphere, J. Atmos. Sci., 41, 351–362, doi:http://dx.doi.org/10.1175/1520-0469(1984)041<0351:OOWMFI>2.0.CO;2, 1984.

Hassler, B., Bodeker, G. E., Solomon, S., and Young, P. J.: Changes in the polar vortex: Effects on Antarctic total ozone observations at various stations, Geophys. Res. Lett., 38, L01805, doi:10.1029/2010GL045542, 2011.

830

Hio, Y. and Hirota, I. Interannual variations of planetary waves in the Southern Hemisphere stratosphere. J. Meteorol. Soc. Jap., 80, 1013–1027, 2002.

Hio, Y. and Yoden, S.: Quasi-periodic variations of the polar vortex in the Southern Hemisphere due to wave-wave interaction, J. Atmos. Sci., 61, 2510–2527, doi:http://dx.doi.org/10.1175/JAS3257.1, 2004.

835

Hirota, I. and Hirooka, T.: Normal mode Rossby waves observed in the upper stratosphere. Part I: First symmetric modes of zonal wavenumbers 1 and 2, J. Atmos. Sci., 41, 1253–1267, doi:http://dx.doi.org/10.1175/1520-0469(1984)041<1253:NMRWOI>2.0.CO;2. 1984.

Hoppel, K., Bevilacqua, R., Allen, D., Nedoluha, G., and Randall, C.: POAM III observation of the anomalous 2002 Antarctic ozone hole, Geophys. Res. Lett., 30, 1394, doi:10.1029/2003GL016899, 2003.

840

Huth, R. and Canziani, P. O.: Classification of hemispheric monthly mean stratospheric potential vorticity fields, Ann. Geophys., 21, 805–817, doi:10.5194/angeo-21-805-2003, 2003.

Ialongo, I., Sofieva, V., Kalakoski, N., Tamminen, J., and Kyrölä, E.: Ozone zonal asymmetry and planetary wave characterization during Antarctic spring, Atmos. Chem. Phys., 12, 2603–2614, doi:10.5194/acp-12-2603-2012, 2012.

845

Kalnay, E., Kanamitsu, M., Kistler, R., Collins, W., Deaven, D., Gandin, L., Iredell, M., Saha, S., White, G., Woollen, J., Zhu, Y., Chelliah, M., Ebisuzaki, W., Higgins, W., Janowiak, J., Mo, K. C., Ropelewski, C., Wang, J., Leetmaa, A., Reynolds, R., Jenne, R., and Joseph, D.: The NCEP/NCAR 40-year Reanalysis Project, Bull. Amer. Meteorol. Soc., 77, 1057–1072, doi:http://dx.doi.org/10.1175/1520-0477(1996)077<0437:TNYRP>2.0.CO;2, 1996.

850

Kodera, K. and Yamazaki, K.: A possible influence of sea surface temperature variation on the recent development of ozone hole, J. Meteorol. Soc. Jpn., 67(3), 465–472, 1989.

Kondragunta, S., Flynn, L. E., Neuendorffer, A., Miller, A. J., Long, C., Nagatani, R., Zhou, S., Beck, T., Beach, E., McPeters, R., Stolarski, R., Bhartia, P. K., DeLand, M. T., and Huang, L.-K.: Vertical structure of the anomalous 2002 Antarctic ozone hole, J. Atmos. Sci., 52, 801–811, doi:http://dx.doi.org/10.1175/JAS-3324.1, 2005.

855

Kuttippurath, J., Lefèvre, F., Pommereau, J.-P., Roscoe, H. K., Goutail, F., Pazmiño, A., and Shanklin, J. D.: Antarctic ozone loss in 1979–2010: first sign of ozone recovery, Atmos. Chem. Phys., 13, 1625–1635, doi:10.5194/acp-13-1625-2013, 2013.

Li, X., Holland, D. M., Gerber, E. P., and Yoo, C.: Impacts of the north and tropical Atlantic Ocean on the Antarctic Peninsula and sea ice, Nature, 505, 538–542, doi:10.1038/nature12945, 2014.

Lin, P., Fu, Q., Solomon, S., and Wallace, J. M.: Temperature trend patterns in Southern Hemisphere high latitudes: Novel indicators of stratospheric change, J. Climate, 23, 4264–4280, doi:10.1175/2009JCLI2971.1, 2010.

Lin, P., Fu, Q., and Hartmann, D. L.: Impact of tropical SST on stratospheric planetary waves in the Southern Hemisphere, J. Climate, 25. 5030–5046, doi:10.1175/JCLI-D-11-00378.1, 2012.

Malanca, F. E., Canziani, P. O., and Argüello, G. A.: Trends evolution of ozone between 1980 and 2000 at midlatitudes over the Southern Hemisphere: Decadal differences in trends, J. Geophys. Res., 110, D05102, doi:10.1029/2004JD004977, 2005.

Marshall, G. J.: Trends in the Southern Annular Mode from observations and reanalyses, J. Climate, 16, 4134–4143, doi:http://dx.doi.org/10.1175/1520-0442(2003)016<4134:TITSAM>2.0.CO;2, 2003.

McPhaden, M. J.: Evolution of the 2002/03 El Niño, Bull. Amer. Meteorol. Soc., 85, 677–695, doi:http://dx.doi.org/10.1175/BAMS-85-5-677, 2004.

Mo, K. C. and Higgins, R. W.: The Pacific-South American modes and tropical convection during the Southern Hemisphere winter, Mon. Wea. Rev., 126, 1581–1596, doi:http://dx.doi.org/10.1175/1520-0493(1998)126<1581:TPSAMA>2.0.CO;2, 1998.

Newman, P. A. and Nash, E. R.: The unusual Southern Hemisphere stratosphere winter of 2002, J. Atmos. Sci., 62, doi: http://dx.doi.org/10.1175/JAS-3323.1, 614–628, 2005.

Newman, P. A., Kawa, S. R., and Nash E. R.: On the size of the Antarctic ozone hole, Geophys. Res. Lett., 31, doi:10.1029/2004GL020596, 2004.

Nishii, K. and Nakamura, H.: Tropospheric influence on the diminished Antarctic ozone hole in September 2002, Geophys. Res. Lett., 31, doi:10.1029/2004GL019532, 2004.

Peters, D. and Vargin, P.: Influence of subtropical Rossby wave trains on planetary wave activity over Antarctica in September 2002, Tellus, 67A, 25875, http://dx.doi.org/10.3402/tellusa.v67.25875, 2015.

Peters, D., Vargin, P., and Körnich, H.: A study of the zonally asymmetric tropospheric forcing of the austral vortex splitting during September 2002, Tellus, 59A, 384–394, doi: 10.1111/j.1600-0870.2007.00228.x, 2007.

Quintanar, A. I. and Mechoso, C. R.: Quasi-stationary waves in the Southern Hemisphere. Part I: Observational data, J. Climate, 8, 2659–2672, doi:http://dx.doi.org/10.1175/1520-0442(1995)008<2659:QSWITS>2.0.CO;2, 1995.

Randel, W. J.: The seasonal evolution of planetary waves in the southern hemisphere stratosphere and troposphere, Q. J. Roy. Meteorolog. Soc., 114, 1385–1409, doi:10.1002/qj.49711448403, 1988.

Raphael, M. N.: A zonal wave 3 index for the Southern Hemisphere, Geophys. Res. Lett., 31, L23212, doi:10.1029/2004GL020365, 2004.

Raphael, M. N., Marshall, G. J., Turner, J., Fogt, R. L., Schneider, D., Dixon, D. A., Hosking, J. S., Jones, J. M., and Hobbs, W. R.: The Amundsen Sea Low: Variability, change, and impact on Antarctic climate, Bull. Amer. Meteorol. Soc., 97, 111–121, doi:10.1175/BAMS-D-14-00018.1, 2016.

Roscoe, H. K., Feng, W., Chipperfield, M. P., Trainic, M., and Shuckburgh, E. F.: The existence of the edge region of the Antarctic stratospheric vortex, J. Geophys. Res., 117, D04301, doi:10.1029/2011JD015940, 2012.

Salby, M., Titova, E., and Deschamps, L.: Rebound of Antarctic ozone, Geophys. Res. Lett., 38, L09702, doi:10.1029/2011GL047266, 2011.

Schneider, D. P., Deser, C., and Fan, T.: Comparing the impacts of tropical SST variability and polar stratospheric ozone loss on the Southern Ocean westerly winds, J. Climate, 28, 9350–9372, doi:10.1175/JCLI-D-15-0090.1, 2015.

Siddaway, J. M., Petelina, S. V., Karoly, D. J., Klekociuk, A. R., and Dargaville, R. J.: Evolution of Antarctic ozone in September–December predicted by CCMVal-2 model simulations for the 21st century, Atmos. Chem. Phys., 13, 4413–4427, doi:10.5194/acp-13-4413-2013, 2013.

Solomon, S., Ivy D. J., Kinnison, D., Mills, M. J., Neely III, R. R., and Schmidt, A.: Emergence of healing in the Antarctic ozone layer, Science, 353(6296), 269–274, doi:10.1126/science.aae0061, 2016.

Solomon, S.: Stratospheric ozone depletion: a review of concepts and history, Rev. Geophys., 37, 275–316, doi:10.1029/1999RG900008, 1999.

Solomon, S., Portmann, R. W., Sasaki, T., Hofmann, D. J., and Thompson, D. W. J.: Four decades of ozonesonde measurements over Antarctica, J. Geophys. Res., 110, D21311, doi:10.1029/2005JD005917, 2005.

Son, S.-W., Purich, A., Hendon, H. H., Kim, B.-M., and Polvani, L. M.: Improved seasonal forecast using ozone hole variability?, Geophys. Res. Lett., 40, 6231–6235, doi:10.1002/2013GL057731, 2013.

925 Stolarski, R. S., Krueger, A. J., Schoeberl M. R., McPeters, R. D., Newman, P. A., and Alpert, J. C.: Nimbus 7 satellite measurements of the springtime Antarctic ozone decrease, Nature, 322, 808–811, doi:10.1038/322808a0, 1986.

Stone, K. A.: Investigating stratospheric ozone change and associated impacts on circulation and climate, Thesis (PhD), University of Melbourne, http://hdl.handle.net/11343/91558, 2015.

930 Stone, K. A., Morgenstern, O., Karoly, D. J., Klekociuk, A. R., French, W. J., Abraham, N. L., and Schofield, R.: Evaluation of the ACCESS – chemistry–climate model for the Southern Hemisphere, Atmos. Chem. Phys., 16, 2401-2415, doi:10.5194/acp-16-2401-2016, 2016.

Thompson, D. W. J., Solomon, S., Kushner, P. J., England, M. H., Grise, K. M., and Karoly, D. J.: Signatures of the Antarctic ozone hole in Southern Hemisphere surface climate change, Nature
935 Geoscience, 4, 741–749, doi:10.1038/NGEO1296, 2011.

Thompson, D. W. J and Wallace, J.: Annular modes in the extratropical circulation. Part I: Month-to-month variability, J. Climate, 13, 1000–1016, doi:http://dx.doi.org/10.1175/1520-0442(2000)013<1000:AMITEC>2.0.CO;2, 2000.

Tully, M. B., Klekociuk, A. R., Deschamps, L. L., Henderson, S. I., Krummel, P. B., Fraser, P. J.,
940 Shanklin, J. D., Downey, A. H., Gies, H. P., and Javorniczky, J.: The 2007 Antarctic ozone hole, Aust. Meteorol. Mag., 57, 279–298, 2008.

Turner, J., Phillips, T., Hosking, J. S., Marshall, G. J., and Orr, A.: The Amundsen Sea low, Int. J. Climatol., 33, 1818–1829, doi:10.1002/joc.3558, 2013.

van der A, R. J., Allaart, M. A. F., Eskes, H. J.: Multi sensor reanalysis of total ozone, Atmos.
945 Chem. Phys., 10, 11277–11294, doi:10.5194/acp-10-11277-2010, 2010.

Varotsos, C.: The Southern Hemisphere ozone hole split in 2002, Environ. Sci. Pollut. Res., 9, 375–376, doi:10.1007/BF02987584, 2002.

Varotsos, C.: What is the lesson from the unprecedented event over Antarctica in 2002? Environ. Sci. Pollut. Res., 10, 80–81, doi:10.1007/BF02980093, 2003a.

950 Varotsos, C.: Why did a "no-ozone-hole" episode occur in Antarctica? Eos, 84, 183–185, doi:10.1029/2003EO190007, 2003b.

Varotsos, C.: The extraordinary events of the major, sudden stratospheric warming, the diminutive Antarctic ozone hole, and its split in 2002, Environ. Sci. Pollut. Res., 11, 405–411, doi:htto://dx.doi.org/10.1065/esor2004.05.205, 2004.

955 Wang, L., Kushner, P. J. and Waugh, D. W.: Southern Hemisphere stationary wave response to changes of ozone and greenhouse gases, J. Climate, 26, 10205–10217, doiI:http://dx.doi.org/10.1175/JCLI-D-13-00160.1, 2013.

Waugh, D. W., Oman, L., Newman, P. A., Stolarski, R. S., Pawson, S., Nielsen, J. E., and Perlwitz, J.: Effect of zonal asymmetries in stratospheric ozone on simulated Southern Hemisphere climate trends, Geophys. Res. Lett., 36, L18701, doi:10.1029/2009GL040419, 2009.

Waugh, D. W. and Randel, W.J.: Climatology of Arctic and Antarctic polar vortices using elliptical diagnostics, J. Atmos. Sci., 56, 1594–1613, doi:http://dx.doi.org/10.1175/1520-0469(1999)056<1594:COAAAP>2.0.CO;2, 1999.

Wirth, V.: Quasi-stationary planetary waves in total ozone and their correlation with lower stratospheric temperature, J. Geophys. Res., 98, 8873–8882, doi:10.1029/92JD02820, 1993.

WMO (World Meteorological Organization): Scientific Assessment of Ozone Depletion: 2014, Global Ozone Research and Monitoring Project, Report No. 55, 416 pp., Geneva, Switzerland, 2014.
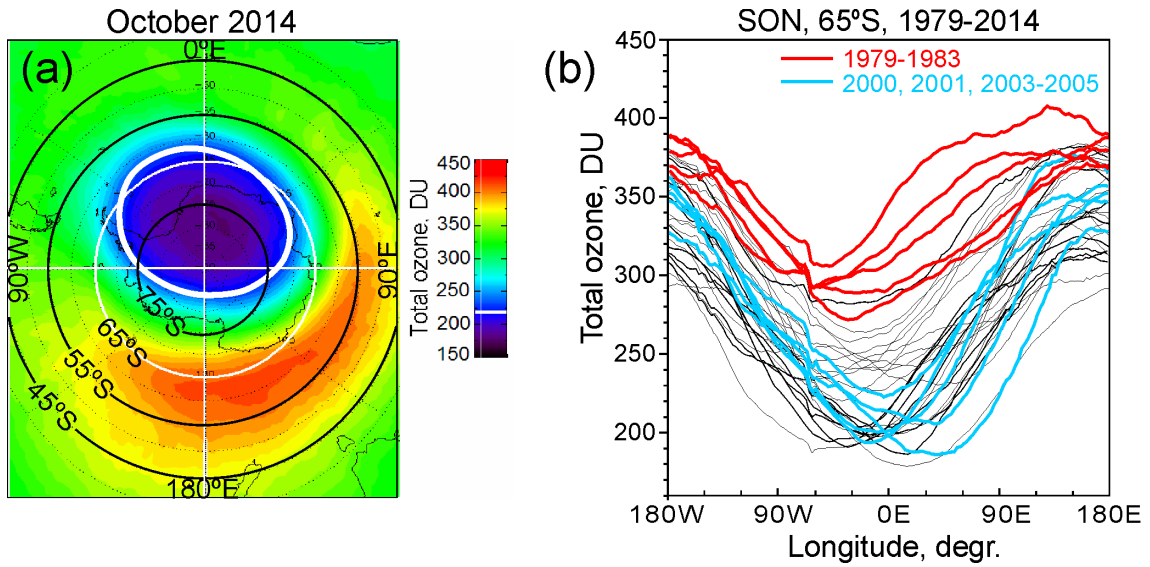
Figure 1: (a) Total ozone in the SH middle/high latitudes in October 2014. (b) Zonal dependence of the total ozone at 65°S averaged for September–November for each year between 1979 and 2014; Red curves show pre-ozone hole years 1979–1983 and blue curves show the years of maximum ozone hole 2000–2005 (apart from the anomalous 2002). Modified from Grytsai et al. (2007a).
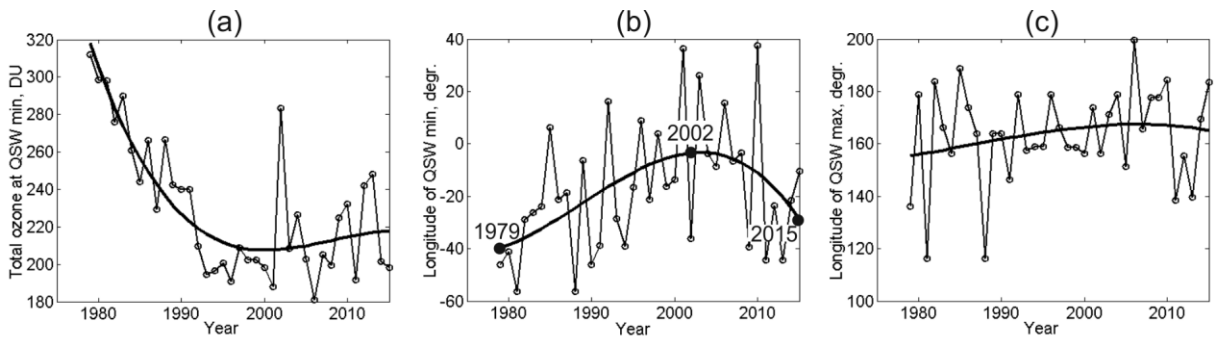
Figure 2: (a) Total ozone at zonal QSW minimum, (b) longitude of QSW minimum and (c) longitude of the QSW maximum at 65°S averaged for September–November. Thin lines are time series of 1979–2015 and thick lines are polynomial fits of degree 3. Longitudes for 1979, 2002 and 2015 from polynomial fitting are marked in (b) by closed circles.
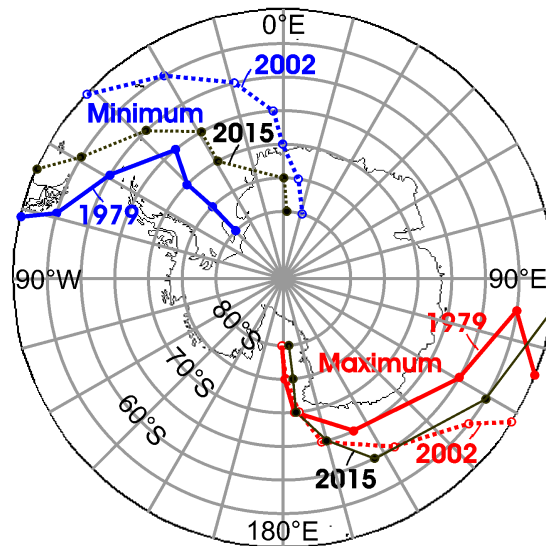
990

Figure 3: Map of longitudinal locations of zonal QSW maximum (red) and zonal QSW minimum (blue) at seven latitudes between 50°S and 80°S; westernmost (easternmost) longitudes in 1979 (2002) determined from the polynomial fit, as shown in Fig. 2b, relate to thick (thin) lines. Black dotted line marks longitudes for 2015. Modified from Grytsai et al. (2007a).

995
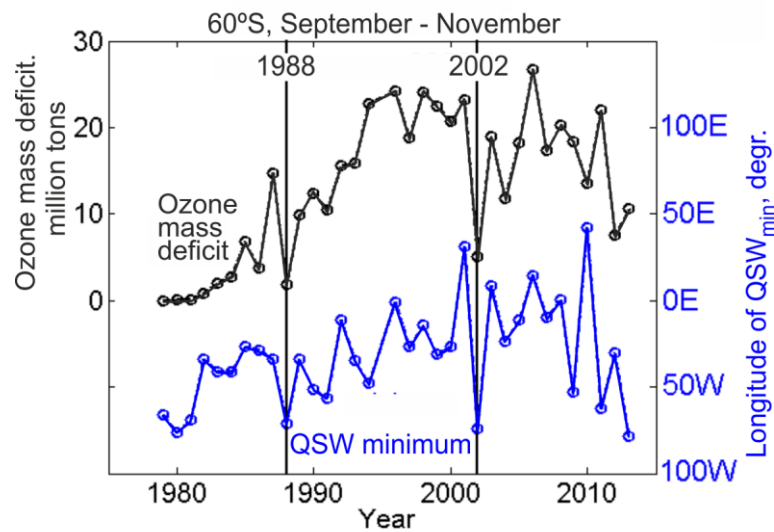
Figure 4: Ozone mass deficit and position of the quasi-stationary minimum in the ozone distribution at 60°S averaged over September–November. Pearson correlation coefficient between the two time series is $r = 0.57$. Data for the ozone mass deficit in the SH high latitudes are from http://ozonewatch.gsfc.nasa.gov/meteorology/SH.html. Years of large (1988) and extreme (2002) stratospheric warmings are indicated by vertical lines.

1000

1005
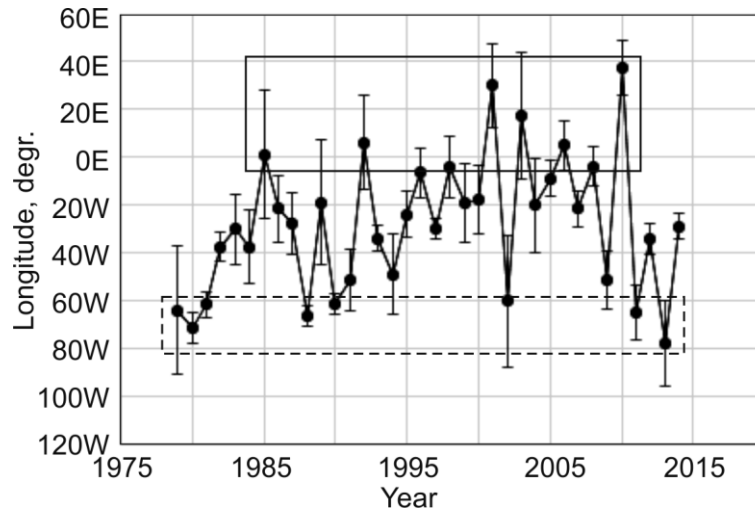
Figure 5: Longitude of MSR TOC ozone minimum (QSW$_{min}$) for SON averaged over four latitudes between 55°S and 70°S, inclusive. The vertical bars span ±1 standard deviation of the individual values used in each average. The solid (dashed) rectangle outlines the upper 80th percentile (lower 20th percentile) corresponding to the maximal eastward (westward) shift of the QSW$_{min}$ longitude.
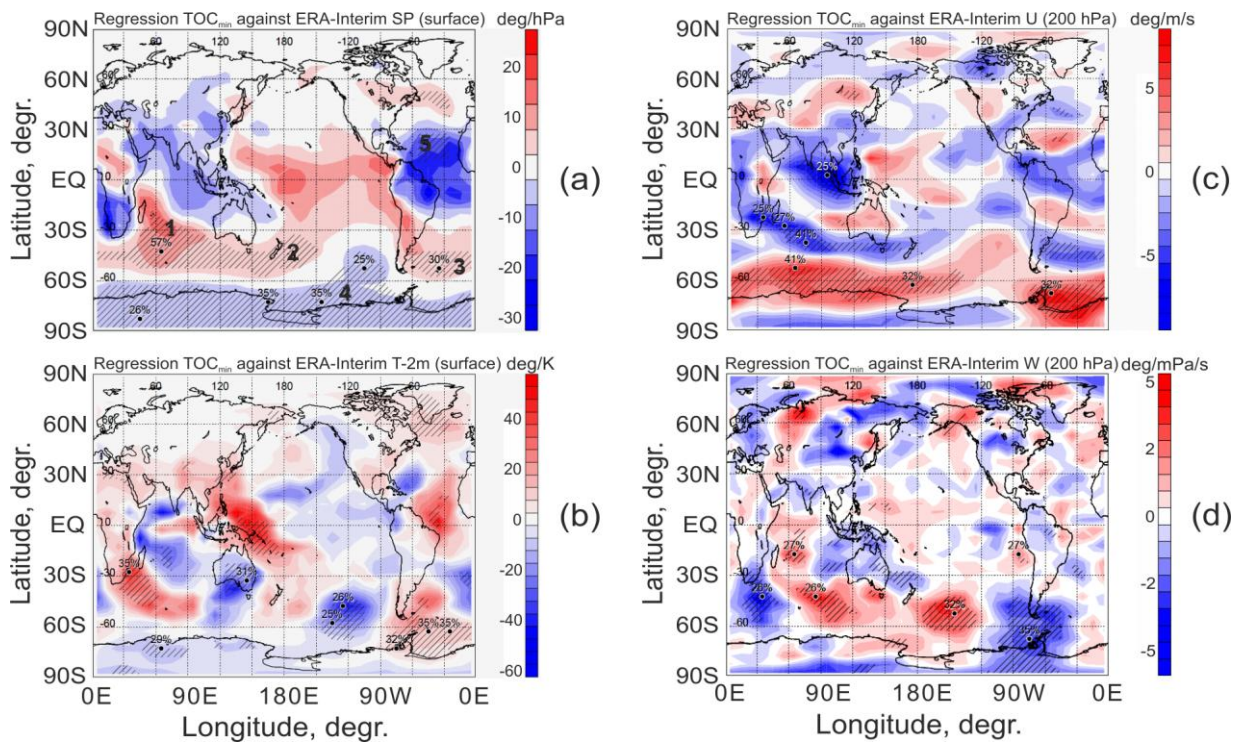
Figure 6: Regression coefficient of the TOC QSW minimum longitude against ERA-Interim climatological anomalies of (a) surface pressure (SP), (b) 2 metre air temperature (T-2m), (c) 200-hPa zonal wind speed (U200) and (d) 200-hPa vertical pressure wind speed (W200) for SON 1979–2014. The units are degrees of longitude per: (a) hPa, (b) K, (c) m s^{-1} and (d) mPa s^{-1}. The hatching is shown where the correlation between the two variables in each panel is significant at the 95% confidence limit.
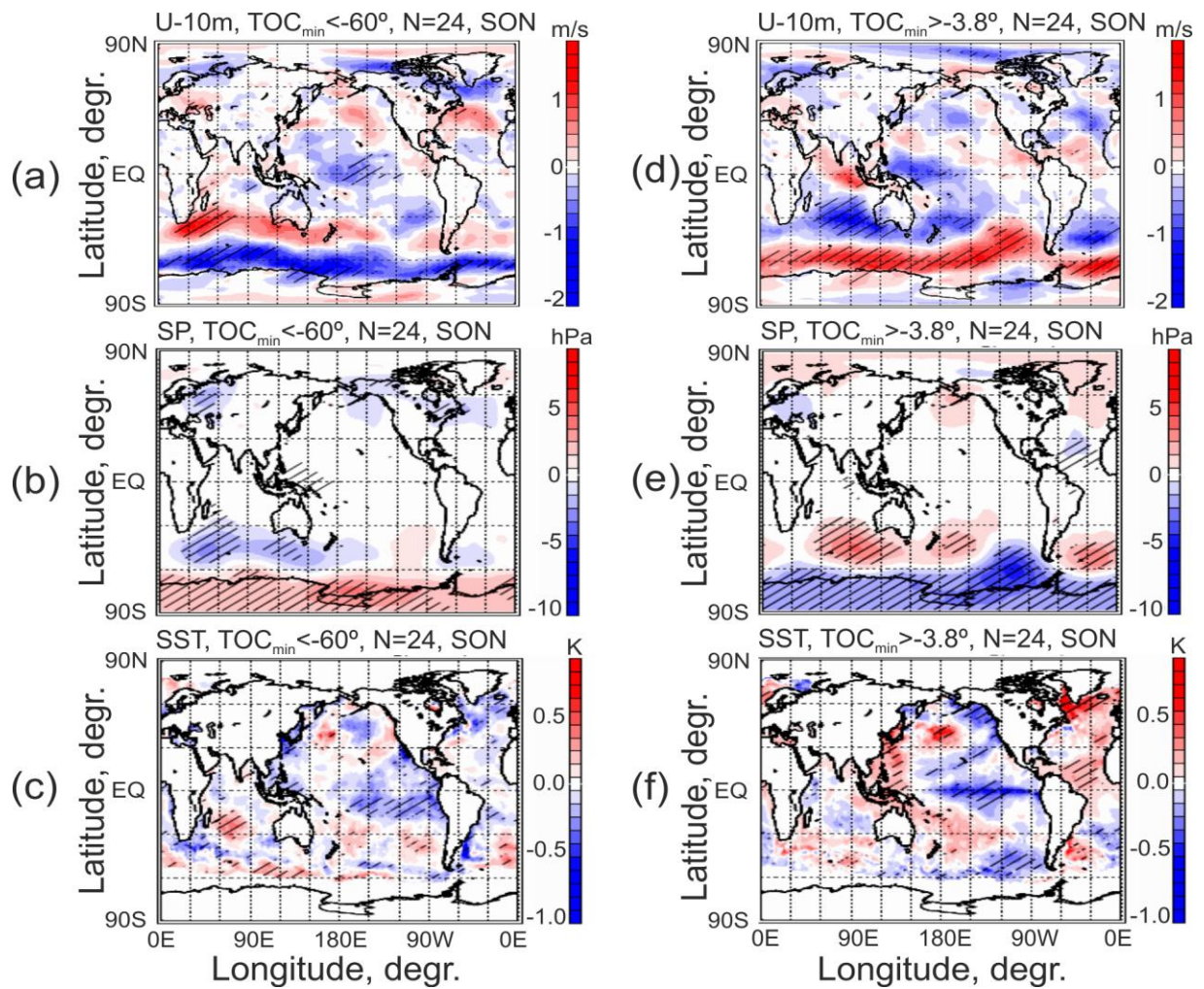
Figure 7: Anomaly composites with respect to the mean climatology for 1979-2014 of ERA-Interim surface meteorological variables for (left) the lower 20th percentile of mean SON QSW_{min} longitudes (western phases) and (right) the upper 80th percentile of mean SON QSW_{min} longitudes (eastern phases). Rows (from top to bottom) are (a, d) 10-m zonal wind (U-10m in m s^{-1}), (b, e) surface pressure (SP in hPa) and (c, f) sea surface temperature (SST in K). Diagonal shading indicates regions significant at the 95% confidence limit (evaluated by comparing the value of each grid box with its standard deviation).
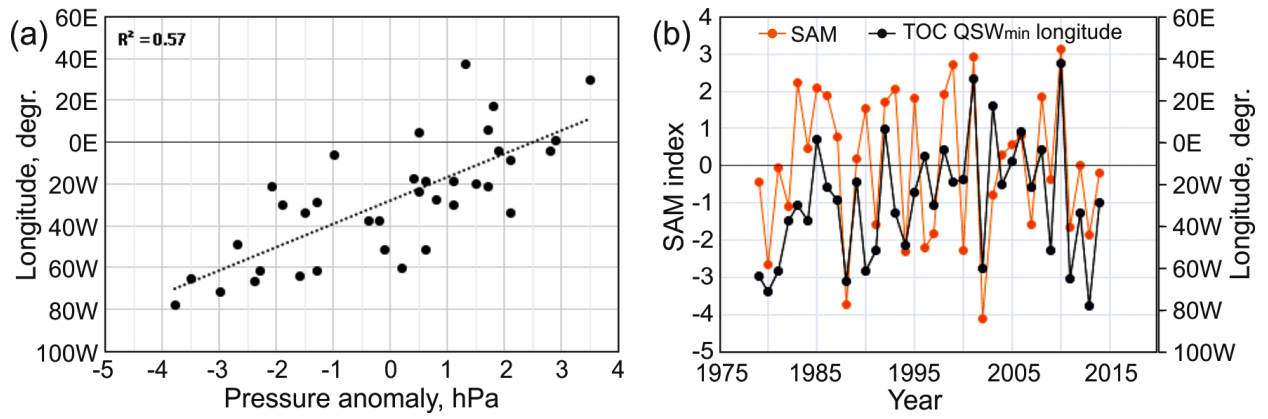
1040

Figure 8: (a) Regression of surface pressure anomaly for grid box 1 (42.5°S, 65.0°E) of Fig. 6a (horizontal axis) against the QSW_{min} longitude (vertical axis). (b) Time series of the standardized SAM index (orange, left axis) and the QSW_{min} longitude (black, right axis). The time series of the QSW_{min} longitude is that shown in Fig. 5. All variables are averaged over September–November. The R^2 value is significant at the 95% confidence limit.
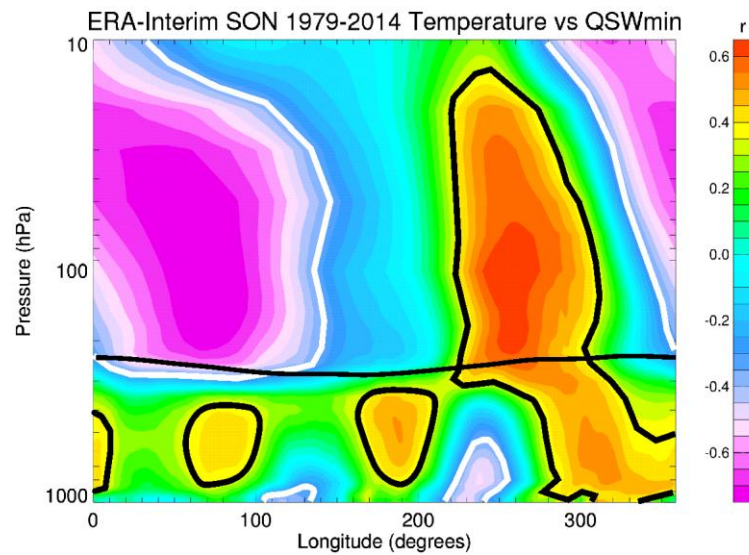
1045
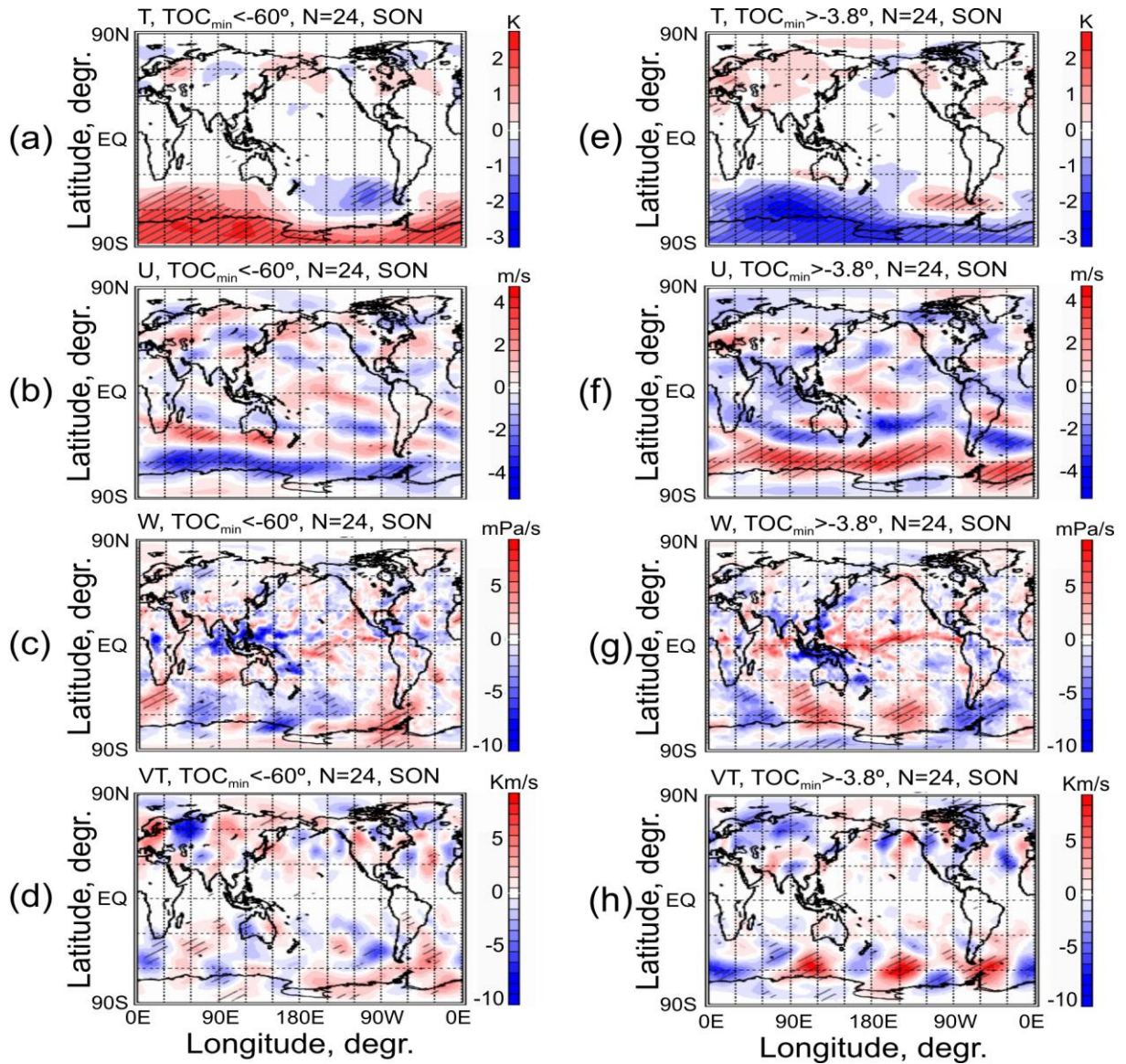
Figure 9: As in Fig. 7, but for ERA-Interim meteorological variables at 200 hPa: (a, e) air temperature (T200 in K), (b, f) zonal wind (U200 in m s^{-1}), (c, g) vertical pressure wind (W200 in mPa s^{-1}), and (d, h) eddy heat flux (V'T' in K m s^{-1}). Diagonal shading indicates as in Figure 7.
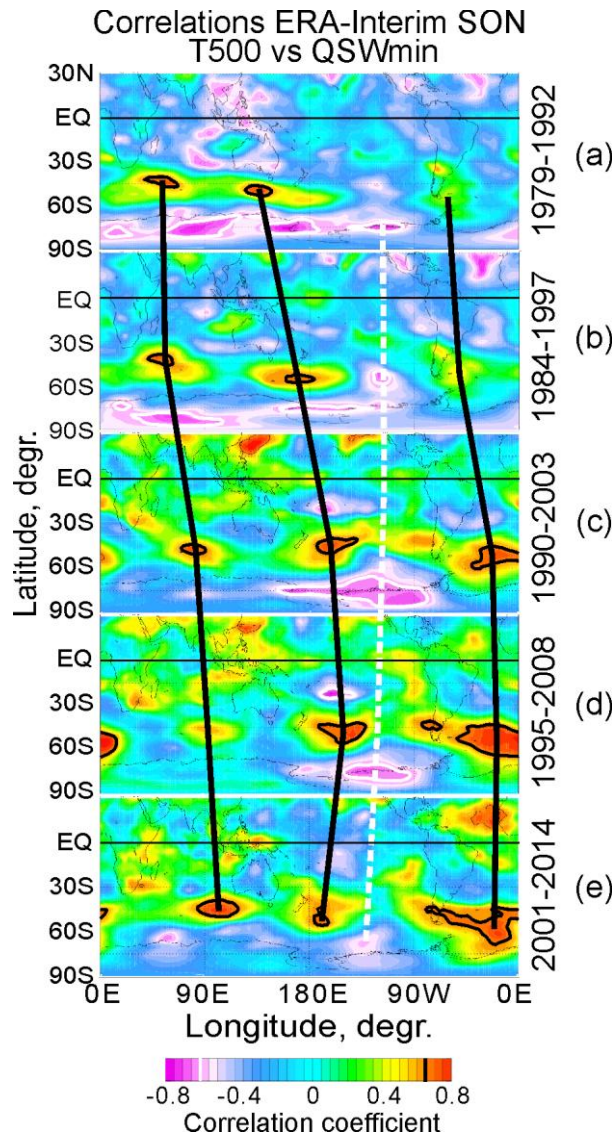
Figure 10: Longitude–height cross-section of the correlation between the QSW_{min} longitude at 65°S and ERA-Interim air temperature averaged over the zone 40–60°S for SON 1979–2014. Thick black curve marks climatological thermal tropopause. Black (white) contours show positive (negative) correlations significant at the 95% confidence limit.

Figure 11: Correlation between the QSW_{min} longitude at 65°S and ERA-Interim air temperature at 500 hPa south of 30°N. Five sequential 14-year intervals with 5-6-year step are presented. Black (white) contours show positive (negative) correlation peaks $r = 0.65$ significant at the 99% confidence limit. Thick solid black (dashed white) lines mark mean longitudinal positions of the positive (negative) correlation peaks in the QSW3 structure.
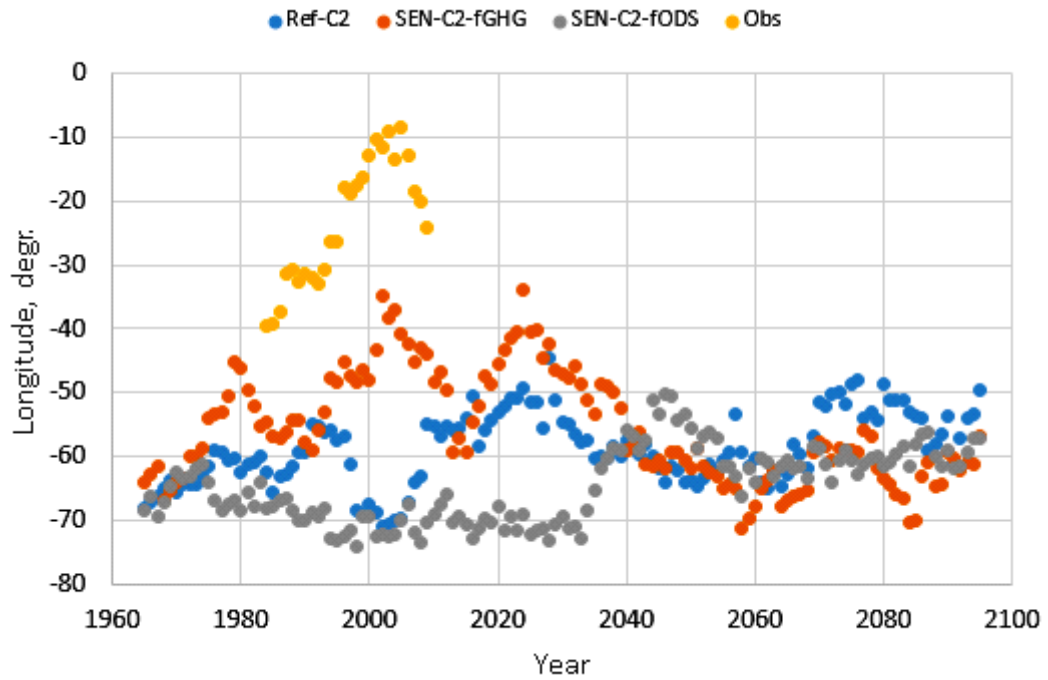
1085 **Figure 12:** Variation of QSW$_{min}$ longitude from the ACCESS-CCM model runs (blue: REF-C2, orange: SEN-C2-fGHG, grey: SEN-C2-fODS) compared with the observations (yellow) shown in Fig. 5. For ACCESS-CCM, the QSW$_{min}$ longitude was obtained by averaging the results for four latitude bands of 5° width between 55°S and 70°S during SON. All time series have been smoothed with an 11 year running mean (i.e. extending from –5 years to +5 years).